Wettability, Hysteresis and Fracture-Matrix Interaction during CO_2 EOR and Storage in Fractured Carbonate Reservoirs

Simeon Agada*, Sebastian Geiger, Florian Doster

Institute of Petroleum Engineering, Heriot-Watt University, Edinburgh, EH14 4AS, United Kingdom

* Corresponding author. Tel.: +44(0) 131 451 8299
E-mail address: simeon.agada@pet.hw.ac.uk

Abstract:

Relative permeabilities show significant dependence on the saturation path during CO_2 enhanced oil recovery (EOR) and Storage. This dependence (or hysteresis) is particularly important for water-alternating-gas (WAG) injection, a successful CO_2 EOR and storage method for clastic and carbonate reservoirs. WAG injection is characterized by an alternating sequence of drainage and imbibition cycles. Hysteresis is hence common and results in residual trapping of the CO_2 phase, which impacts the volume of CO_2 stored and the incremental oil recovery. The competition between hysteresis and geological heterogeneity during CO_2 EOR and storage, particularly in carbonate reservoirs, is not yet fully understood.

In this study, we use a high-resolution simulation model of a Jurassic Carbonate ramp, which is an analogue for the highly prolific reservoirs of the Arab D formation in Qatar, to investigate the impact of hysteresis during CO_2 EOR and storage in heterogeneous carbonate formations. We then compare the impact of residual trapping (due to hysteresis) on recovery to the impact of heterogeneity in wettability and reservoir structure. End-member wettability scenarios and multiple wettability distribution approaches are tested, while, effective fracture permeabilities are computed using discrete fracture networks (DFN), ranging from sparsely distributed background fractures to fracture networks where intensity varies with proximity to faults.

The results enable us to analyse the efficiency of oil recovery and CO_2 sequestration in carbonate reservoirs by comparing the impact of physical displacement processes (e.g., imbibition, drainage, residual trapping) and heterogeneous rock properties (e.g., wettability, faults, fractures, layering) that are typical in carbonate reservoirs. We show that although the fracture network properties have the greatest impact on the fluid flow, the effect of wettability and hysteresis is nontrivial. Our results emphasise the need for wettability to be accurately measured and appropriately distributed in a reservoir simulation model. Similarly, our results indicate that hysteresis effects in cyclic displacement processes must be accounted for in detail to ensure that simulation models give accurate predictions.

Keywords:

Wettability, Hysteresis, Residual Trapping, CO2 EOR and Storage, Discrete Fracture Network

1. Introduction

Carbon capture and storage (CCS) in subsurface reservoirs can potentially contribute to reducing CO_2 emissions and mitigating global climate change (e.g., Qi et al., 2009; Jenkins et al., 2012; Liu et al., 2012; Szulczewski et al., 2012; Petvipusit et al., 2014; Wriedt et al., 2014). CCS can be implemented simultaneously with CO_2 enhanced oil recovery (EOR) to achieve mutual benefits of subsurface CO_2 storage and increased oil production in depleted hydrocarbon fields. Oil reservoirs are particularly attractive for CO_2 storage because the geology is relatively well known thereby reducing geological uncertainties associated with CO_2 migration and geological storage (Kovscek, 2002; Kovscek and Cakici, 2005; Iding and Ringrose, 2010; Leach et al., 2011; Sohrabi et al., 2011; Liu et al., 2012; Ettehadtavakkol et al., 2014; Azzolina et al., 2015).

Carbonate reservoirs which are estimated to contain about 60% of global conventional and unconventional hydrocarbon resources (Beydoun 1998; Burchette, 2012; Agar and Geiger, 2015) form suitable candidates for CO_2 EOR and storage because of the potentially large amounts of CO_2 that can be sequestered in carbonate formations while improving hydrocarbon recovery (Liu et al., 2012). Carbonate reservoirs, however, are often difficult to exploit due to multiscale heterogeneities that arise from complex diagenetic, reactive, depositional and deformational processes, resulting in complicated subsurface flow behaviours. Carbonate reservoirs may also contain multiscale natural fracture networks that comprise complex high permeability flow paths in the reservoir (e.g., Guerreiro et al., 2000; Gale et al., 2004; Toublanc et al., 2005; Belayneh and Cosgrove, 2010). The variability in matrix structure and fracture network connectivity is the main reason why fractured carbonate reservoirs show a large variety of flow behaviours, leading to **s**ignificant uncertainties in predicting CO_2 plume distributions and hydrocarbon recovery (Cosentino et al., 2001; Bourbiaux et al., 2002; Makel, 2007).

The reliability of underground CO_2 storage during EOR in fractured carbonate reservoirs depends on a number of interrelated trapping mechanisms. Structural trapping defines the geometry of the store within which more permanent storage can occur. Solubility trapping occurs when CO_2 dissolves into the formation brine. Mineral trapping which entails geochemical binding of CO_2 to the rock due to mineral precipitation, guarantees permanent

CO_2 immobilisation but on a scale of hundreds to thousands of years, too long to have a bearing on storage security over an operational period. Residual trapping is due to snap-off (or disconnection) of the CO_2 phase such that it becomes an immobile (trapped) phase when droplets of CO_2 become isolated from the CO_2 plume by encroaching brine (Juanes et al., 2006). Residual trapping occurs due to differences in the advancing and receding contact angles during repeat imbibition and drainage cycles. It is this sequestration mechanism, residual trapping, which occurs over years to decades (short-term storage), that we investigate in this study. Understanding the underlying physicochemical processes responsible for residual trapping can therefore provide a conservative estimate of CO_2 storage security over timescales in line with EOR projects (Bachu et al., 1994; Pruess et al., 2003; Juanes et al., 2006; Qi et al., 2008, 2009; Wilkinson et al., 2009; Burnside and Naylor, 2014).

We focus on the relationship between residual trapping of CO_2 and water-alternating-gas (WAG) injection which has been found to be a successful EOR mechanism for carbonate reservoirs (Christensen et al., 2001; Manrique et al., 2007; Awan et al., 2008; Kalam et al., 2011; Pizarro and Branco, 2012; Rawahi et al., 2012). CO_2 WAG injection combines the benefits of gas injection to reduce the residual oil saturation and water injection to improve mobility control and frontal stability (Fig. 1). Due to the cyclic nature of CO_2 WAG injection, hysteresis is common and leads to the residual trapping of CO_2. Hysteresis occurs as a result of the dependence of **r**elative permeability and capillary pressure curves on the saturation history (Fig. 2). Only hysteresis models are able to capture the overall benefit of residual trapping, which lies in the fact that it can safely trap CO_2 in the subsurface while reducing the overall CO_2 phase mobility and improving enhanced oil recovery estimates (Spiteri and Juanes, 2006; Burnside and Naylor, 2014).

Several models have been developed to account for hysteresis during multiphase flow in subsurface reservoirs. They are based on the use of scanning curves in which the direction of saturation change is reversed at a number of intermediate saturations. Killough's (1976) two-phase hysteresis model accounts for hysteresis as a function of the Land trapping parameter (Land, 1968). This model allows for reversibility of drainage and imbibition cycles along the same scanning curve. Carlson's (1981) model accounts for hysteresis by predicting the trapped non-wetting phase saturation via shifting of the bounding imbibition curve.

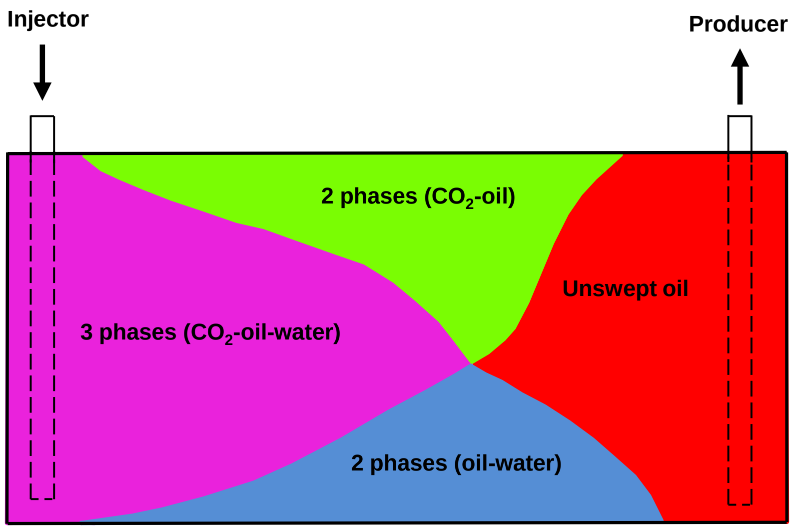

Fig. 1. Conceptual model of immiscible CO_2 WAG injection. Water and CO_2 are injected through same well, generating two- and three-phase regions. CO_2 WAG injection combines the benefits of gas injection to reduce the residual oil saturation and water injection to improve mobility control and frontal stability.

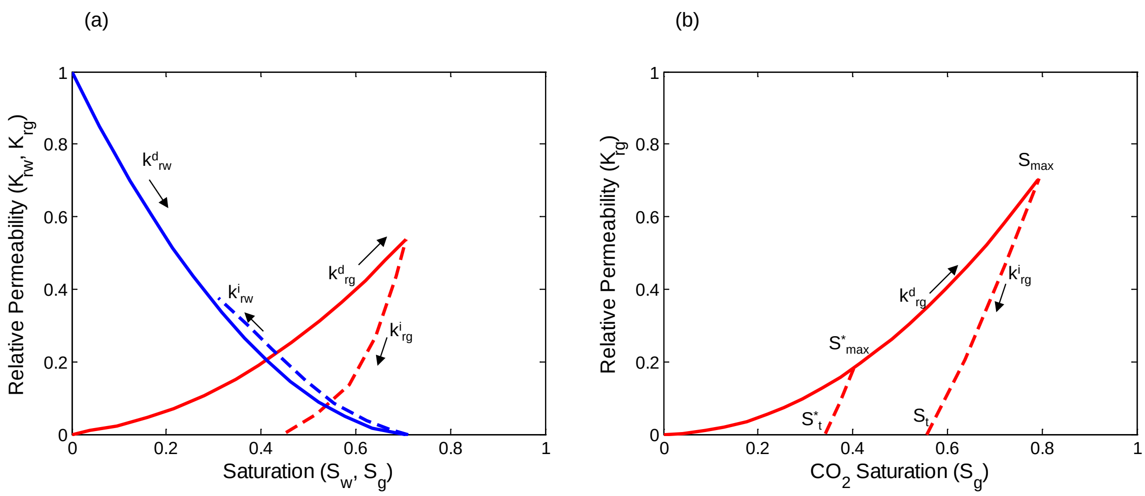

Fig. 2. Relative permeability curves (a, b) illustrating hysteresis and residual CO_2 trapping during WAG injection. Hysteresis effect is more significant for the non-wetting CO_2 phase (a). Scanning curves illustrate the maximum trapped fraction (S^*_t, S_t) corresponding to the maximum CO_2 saturation (S^*_{max}, S_{max}) at flow reversal (b). Superscripts *d* and *i* refer to drainage and imbibition respectively.

The Carlson (1981) model, which also employs reversible scanning curves, is only adequate if the intermediate scanning curves are almost parallel and the imbibition curve has minimal curvature. Three-phase hysteresis models have been developed that represent non reversibility (or cycle dependence) of scanning curves during hysteresis (e.g. Lenhard and Parker, 1987; Lenhard and Oostrom, 1998; Larsen and Skauge, 1998; Egermann et al., 2000; Shahverdi et al., 2014; Beygi et al., 2015) and are thought to include the essential flow physics during cyclic flooding. Furthermore, detailed numerical models which represent hysteresis mechanisms at the pore scale (e.g., Blunt et al., 2002; Jackson et al., 2003; Joekar-Niasar et al., 2008, 2012) can increase our understanding of the pore scale physics of hysteresis and residual trapping during cyclic displacement processes.

Hysteresis is also influenced by wettability. Knowledge of the wetting preference and its variation in a carbonate reservoir rock is fundamental to understanding flow behaviour during CO_2 EOR and storage but is difficult to quantify due to the intrinsic heterogeneity of carbonates (Okasha et al., 2007; Ferno et al., 2011; Dernaika et al., 2013). Several authors (e.g., Kovscek et al., 1993; Jadhunandan and Morrow, 1995; Blunt, 1997; Hui and Blunt, 2000; van Dijke et al., 2001; Al-Futaisi and Patzek, 2003; Valvatne and Blunt, 2004; Ryazanov et al., 2009, 2010) have demonstrated how wettability changes alter relative permeability functions, using a number of drainage and imbibition simulations and experiments where the range of advancing and receding contact angles was modified. They found that during imbibition, the transport properties of permeable porous media are sensitive to the hysteresis between receding and advancing contact angles. This difference ultimately controls the amount of trapped fluids due to hysteresis and needs to be captured in reservoir simulation models.

The aim of this study is to investigate the effect of residual trapping (due to hysteresis) on CO_2 EOR and storage in relation to the multiscale heterogeneities that are pervasive in fractured carbonate reservoirs. Residual trapping is demonstrated using hysteresis models with reversible scanning curves during WAG imbibition and drainage cycles. In the context of WAG, we use the following notation for the remainder of the paper. The term "imbibition" refers to the displacement of gas by increasing gas saturation while the term "drainage" refers to the displacement of liquid by increasing gas saturation.

The fracture system is represented with discrete fracture network (DFN) models generated using detailed geological observations. The DFN is then upscaled to obtain effective permeability tensors for the fracture grid that is coupled to the matrix using a dual-porosity dual-permeability model. Because the specific geometry of the DFN is difficult to constrain, we investigate three distinct hypotheses for the evolution of the fracture system; (1) Regional fracture geometry which represents a pervasive background fracture system (2) Fault related fracture geometry where fractures cluster around faults and decrease in intensity as the distance to faults increase (3) Bedding related fracture geometry where the fractures are stratigraphically confined to the bedding and give rise to high fracture permeability layers.

Since the structural, multiphase flow and transport properties encountered in the reservoir exhibit such significant uncertainties, we use multiple numerical simulations to analyse the following questions: How can we improve our understanding and prediction of subsurface flow behaviour during CO_2 EOR and storage under geological uncertainty? By investigating the range of uncertainties in wettability, residual trapping and the fracture network, can we rank their impact on the efficiency of CO_2 EOR and storage in fractured carbonate formations? What engineering measures can be used to mitigate the effect of geological uncertainties? Can we use our workflow to screen different CO_2 EOR and storage projects, determine the best solutions for specific reservoirs and identify optimum CO_2 EOR and sequestration strategies? Is there a competition between maximising CO_2 EOR and maximising CO_2 storage?

2. Setup of Numerical Simulation Models

2.1 Geological description of the fractured carbonate reservoir

This study is based on a flow simulation model constructed for the Amellago Island Outcrop, a Jurassic carbonate ramp in the High Atlas Mountains of Morocco in North Africa (Fig. 3). The outcrop is an analogue for one of the most important carbonate formations in the Middle East, the Arab D formation in Qatar (Pierre et al., 2010; Amour et al., 2013; Agada et al., 2014). Significant structural and lithological heterogeneity was observed in the outcrop including sub-seismic faults and fractures. The influence of faults is most notable in the extent to which fault-zone materials affect cross-fault flow. Where there is significant cementation within the fault and/or fault-zones, the faults may act as seals or baffles that compartmentalize the reservoir. Otherwise, the juxtaposition of high and low permeability layers due to displacement across the faults may limit but not totally impede cross-fault flow. Other geological features captured in the matrix of the flow simulation model include oyster bioherms, mud mounds, diagenetic hard-grounds and channelling. A detailed description of the geological modelling, upscaling, dynamic model construction and permeability distribution for the Amellago outcrop analogue reservoir is presented in Agada et al. (2014).

2.2 Matrix Simulation Model

The flow simulation model (Fig. 3) which captures key structural and sedimentological heterogeneities observed in the Amellago Island outcrop is discretized into 74 x 75 x 36 grid cells (199,800 grid cells in total) and has dimensions of 1.15 x 1.17 x 0.11 km. Permeability and porosity for the facies in the outcrop were modelled using data from real subsurface reservoirs to ensure a realistic distribution of reservoir quality. At the reservoir model grid-block scale, the matrix porosity varies from 0.01% to 38% while the matrix permeability varies from 0.01 mD to 855 mD (Fig. 4). WAG injection was simulated using 10 alternating cycles during which 0.075 PV of water followed by 0.075 PV of gas was injected per cycle. The WAG ratio was set to 1:1 and the cycle length to 1 year to ensure proper gravity segregation of injected fluids. A regular five-spot well pattern was used with a vertical producer at the centre of the model and four vertical injectors situated at the corners of the model. The injector-producer spacing was approximately 400 m and the wells were completed across the entire reservoir interval. The injectors were set to operate at target liquid rate subject to a maximum bottom-hole pressure (BHP) constraint of 41,369 kPa, while the producer was set to operate at a target liquid rate subject to a minimum BHP of 16,547 kPa. These pressures were specified to ensure that a pressure gradient of 11-45 kPa/m was encountered in the reservoir model at all times. The reservoir was assumed to have an isothermal reservoir temperature of 121°C, an initial reservoir pressure of 20,684 kPa and a bubble point pressure of 11,367 kPa. The reference densities of water, oil and CO_2 were set to 1000 kg/m^3, 800 kg/m^3 and 1.35 kg/m^3 respectively, while, the reference viscosities of water, oil and CO_2 were set to 0.31 cp, 0.52 cp and 0.02 cp respectively.

All simulations have been carried out using the black oil simulator IMEX (CMG). The black oil model represents the multi-phase multi-component system of reservoir fluids through three pseudo components: water, oil and gas. These three components form three phases: an aqueous phase that only consists of the water component, a gas phase that consists only of the gas component, and an oil phase that is formed by oil but dissolves gas. The density and viscosity of the oil phase depend on its composition (Dake, 1998). In this study, we address CO_2 EOR and storage and hence assign CO_2 properties to the gas phase and component. The black oil model limits the overall computational cost while allowing us to represent features of interest including mass conservation, buoyancy, viscosity alteration, hysteretic phenomena, fracture-matrix exchange and relatively large spatial domains. Our approach is consistent with previous studies which have used the black oil model to investigate CO_2 EOR and/or CO_2 storage in geological reservoirs (e.g., Egermann et al., 2000; Jessen et al., 2005; Juanes et al., 2006; Spiteri and Juanes, 2006; Benisch and Bauer, 2013; Petvipusit et al., 2014).

In order to complete the entire study within a realistic time frame, we make a few simplifying assumptions that allow us to investigate the interactions between the features of interest and provide insights on the flow dynamics during CO_2 EOR and Storage. First, we focus on displacement scenarios where the reservoir pressure is below the minimum miscibility pressure (MMP) and as such oil and CO_2 are immiscible. Secondly, we do not consider the effects of physical dispersion which for large scale displacement processes is often minimal and/or masked by numerical dispersion. Thirdly, we represent two-phase and three-phase relative permeability and capillary pressures with standard models (i.e. the Corey and Stone models, respectively, see below) that are available in IMEX.

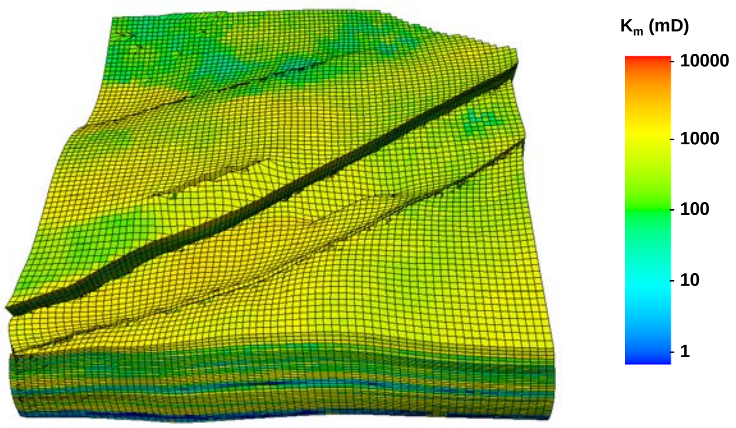

Fig. 3. Matrix simulation model of the Amellago Island Outcrop, showing the horizontal permeability distribution. The model dimensions are 1.15 x 1.17 x 0.11 km. Individual grid blocks have dimensions of 15x15x3m.

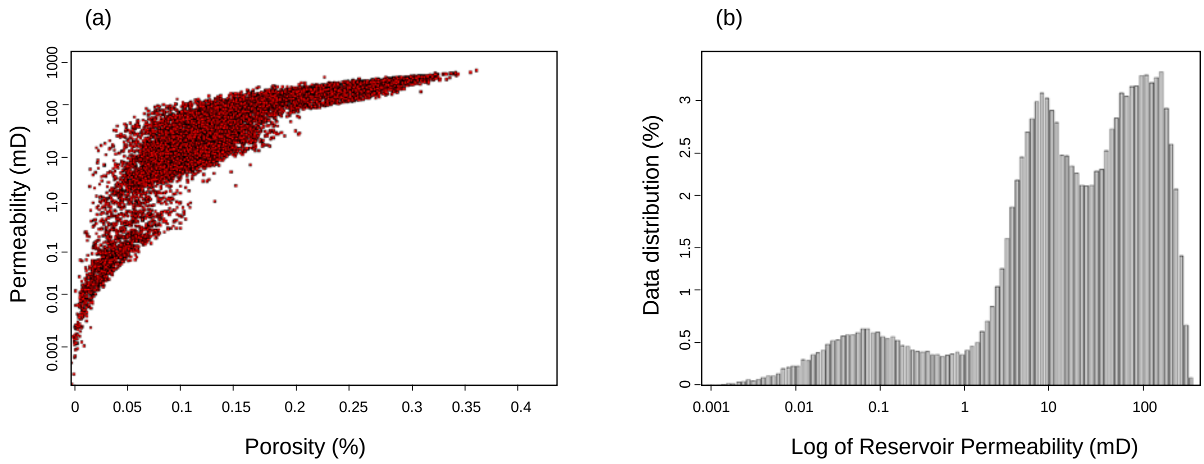

Fig. 4. Porosity-Permeability distribution (a) and permeability histogram (b) for the matrix used in the reservoir simulation model. Note that the data refers to the porosity and permeability values assigned to the reservoir model grid blocks.

For reference, we provide a brief summary of the black oil model equations. A detailed mathematical description of the black oil formulation can be found elsewhere (e.g., Dake, 1998; Chen et al., 2006). Lowercase and uppercase subscripts are used to denote phases and components, respectively. The mass conservation equations for the three components; water, oil, and gas, are given by:

$$\frac{\partial(\phi\rho_w S_w)}{\partial t} = -\nabla.(\rho_w v_w) + q_W \quad (1)$$

$$\frac{\partial\left(\phi\rho_{O_o} S_o\right)}{\partial t} = -\nabla.\left(\rho_{O_o} v_o\right) + q_O \quad (2)$$

$$\frac{\partial}{\partial t}\left(\phi\left(\rho_{G_o} S_o + \rho_g S_g\right)\right) = -\nabla.\left(\rho_{G_o} v_o + \rho_g v_g\right) + q_G \quad (3)$$

for the water, oil and gas components, where, ρ_{G_o} and ρ_{O_o} denote the partial densities of the gas and oil components in the oil phase, respectively. ϕ, ρ, S, v, q represent the porosity, density, saturation, velocity and the source/sink term respectively. These conservation laws are complemented by constitutive equations. The velocities are given by Darcy's law for each phase as:

$$v_\alpha = -\frac{k_{r\alpha}}{\mu_\alpha} K(\nabla P_\alpha - \rho_\alpha \gamma \nabla z), \qquad \alpha = w, o, g, \tag{4}$$

where, K, γ and ∇z denote the total permeability, gravity term and depth respectively. Similarly, k_r, μ and ∇P denote the phase relative permeability, phase viscosity and phase pressure change respectively. The phase pressures are related by capillary pressures, P_c, where:

$$P_{cow} = P_o - P_w, \qquad P_{cgo} = P_g - P_o \tag{5}$$

Furthermore, the whole pore-space is filled by the mixture and hence the contribution of each phase is given by:

$$S_w + S_o + S_g = 1 \tag{6}$$

The complex pore-scale interaction between the individual phases is represented by empirical relationships for capillary pressure and relative permeability. Here, we follow the standard approach and assume that first order effects are captured by algebraic functions that only take saturations as arguments. For two-phase systems, parameterized curves are fitted to experimental data. Here, we use the Corey (1954) parameterizations for relative permeability and capillary pressure which for an oil-water system is given by,

$$k_{rw} = k_{rw,max} \left(\frac{S_w - S_{wi}}{1 - S_{wi} - S_{orw}} \right)^m \tag{7}$$

$$k_{ro} = \left(\frac{1 - S_w - S_{orw}}{1 - S_{wi} - S_{orw}} \right)^n \tag{8}$$

$$P_c = P_{c_{th}} + \left(\frac{1 - S_{wn}}{1 + aS_{wn}}\right)\left(P_{max} - P_{c_{th}}\right) \tag{9}$$

$$S_{wn} = \left(\frac{S_w - S_{wir}}{1 - S_{wir}}\right) \tag{10}$$

where m and n are the Corey exponents for relative permeability to water and oil. $P_{c_{th}}$ denotes the threshold capillary entry pressure, while, a denotes an adjustable constant used to fit experimental data. S_{wn} represents the normalized water saturation. The parameterizations for the oil-gas system follow similarly. The oil-water and gas-oil relative permeability and capillary pressure curves generated with the Corey (1954) formulation were intended to mimic the average behaviour of carbonates such as those discussed in Clerke (2009) and to cover a wide range of wettability scenarios from water-wet to oil-wet (Fig. 5).

Measurement of relative permeability for three-phase systems is time-consuming and very challenging. Therefore, empirical expressions that obtain three-phase relative permeabilities by combining two phase data are commonly employed (e.g., Stone 1970, 1973; Baker, 1988; Blunt, 2000). Here, we use the Stone II interpolation model (Stone, 1973) to compute three-phase relative permeabilities. The Stone II formulation assumes that the functions for the most and least wetting fluid depend only on their saturation and are obtained from the two-phase system with the intermediate wetting fluid. In water-wet reservoirs, water is the most wetting, gas the least wetting and oil the intermediate wetting fluid. In oil-wet reservoirs the role of water and oil are reversed. In a water-wet reservoir the relative permeability to oil is obtained by an interpolation between the relative permeability to oil in an oil-water system and the relative permeability to oil in an oil-gas system. The Stone II model is given by:

$$k_{ro}\left(s_w, s_g\right) = k_{rocw}\left(\frac{k_{row}(s_w)}{k_{rocw}} + k_{rw(s_w)}\right)\left(\frac{k_{rog}(s_g)}{k_{rocw}} + k_{rg}\left(s_g\right)\right) - k_{rw}(s_w) - k_{rg}(s_g),$$

where k_r and S represent the relative permeability and fluid saturation respectively. The subscripts o, w, g and cw represent oil, water, gas and connate-water respectively.

We note that the appropriate representation of three-phase systems is subject to active research including 3D pore-network models that encapsulate laboratory observed microscopic displacement processes (e.g., Blunt, 2000; Piri and Blunt, 2005; Al-Dhahli et al., 2013, 2014) and novel interpolation methods (e.g., Shervadi and Sohrabi, 2012; Beygi et al., 2015). However, for the relatively large spatial domain and volumetric displacement encountered in this study, the simulation results do not change when interpolation models are varied, hence, it was sufficient to use the industry standard Stone II model which is available in IMEX.

While it is common to model relative permeability and capillary pressure as algebraic relations that only depend on the current saturation, it is well established that these functions can depend on the saturation history. We have used the Killough (1976) hysteresis model to account for the path dependency of the relative permeabilities during alternate drainage and imbibition cycles. The Killough model is a computationally efficient approach that sufficiently captures the hysteresis effects encountered in this study. For the relative permeability, the Killough hysteresis model is given by:

$$k_{rg}^{i}(S_g) = k_{rg}^{i}(S_g^*)\frac{k_{rg}^{d}(S_{gi})}{k_{rg}^{d}(S_{gi,max})} \tag{12}$$

where

$$S_g^* = S_{gt,max} + \frac{(S_g - S_{gt})(S_{gi,max} - S_{gt,max})}{S_{gi} - S_{gt}} \tag{13}$$

Capillary pressure curves also exhibit hysteresis effects and several models have been developed to represent capillary pressure hysteresis (e.g., Killough, 1976; Lenhard and Parker, 1987; Lenhard and Oostrom, 1998). In practice, however, capillary pressure hysteretic effects are often negligible when simulating field-scale displacement processes such as in our study where the capillary length is much less than the grid resolution (e.g., Aziz and Settari, 1979; Spiteri and Juanes, 2006; Juanes et al., 2008; Agada et al., 2014).

Hence, we do not consider capillary pressure hysteresis in the current study but refer to Doster et al. (2013a) for a detailed description of capillary pressure hysteresis effects.

Table 1. Main parameters used to generate two-phase relative permeability and capillary pressure curves with Corey equations.

Parameters	Symbol	Wettability		
		Water-wet	Mixed-wet	Oil-wet
Maximum Water Relative Permeability	$K_{rw, max}$	0.20	0.65	0.90
Initial Water Saturation	S_{wi}	0.22	0.10	0.05
Residual Oil Saturation	S_{orw}	0.26	0.15	0.08
Oil Corey Exponent	m	2.50	3.50	4.50
Water Corey Exponent	n	4.50	3.50	2.50
Fitting Constant	a	120	120	120
Maximum Capillary Pressure (kPa)	P_{max}	483	379	276

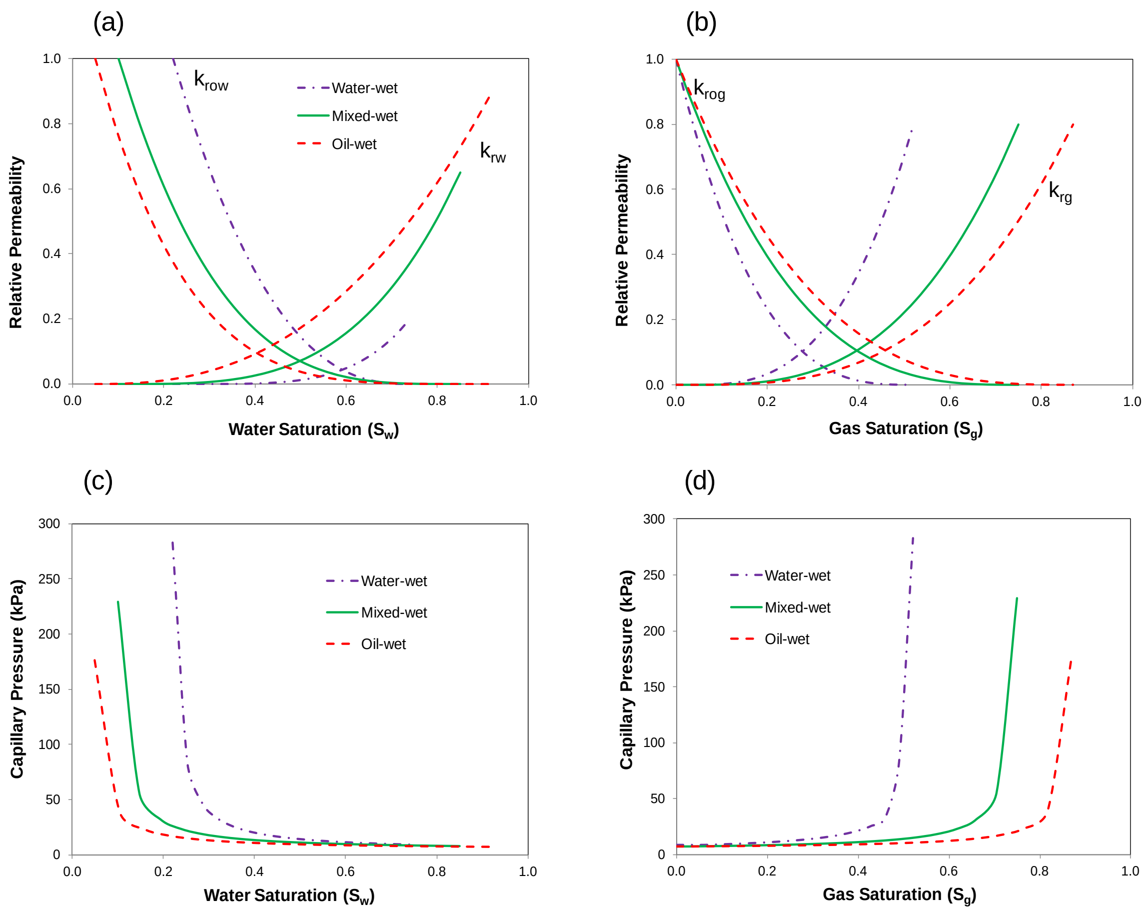

Fig. 5. Relative permeability curves (a, b) and drainage capillary pressure curves (c, d) used in the flow simulations for end-member wettability scenarios.

The common assumption in reservoir simulation studies for the wettability of reservoir rock is that it is constant and water wet. However, wettability typically varies both laterally and vertically. In particular the exposure to oil over geological time-scales may alter the wetting property of a reservoir rock. In this paper, we also address the impact of heterogeneous wetting properties. We compare a depth based distribution approach and a facies based distribution approach to the homogeneous approach. Distributing the wettability on the basis of variation with depth (Fig. 6a) is consistent with the method employed in previous field studies for clastic and carbonate reservoirs (e.g., Jerauld and Rathmell, 1997; Jackson et al., 2003, 2005; Okasha et al., 2007). An alternative method involves distributing the wetting properties by correlating the wettability to the horizontal permeability of individual simulation grid cells (Fig. 6b) based on the facies types (e.g., Clerke, 2009; Agada et al., 2014). We considered multiple wettability distribution approaches because the wettability is only represented in qualitatively adjusted relative permeability and capillary pressure functions to mimic the behaviour of real carbonate reservoirs and the approaches considered seemed to be the most feasible, although, they may be too simplistic for real carbonate reservoirs (Gomes et al., 2008; Hollis et al., 2010; Chandra et al., 2015).

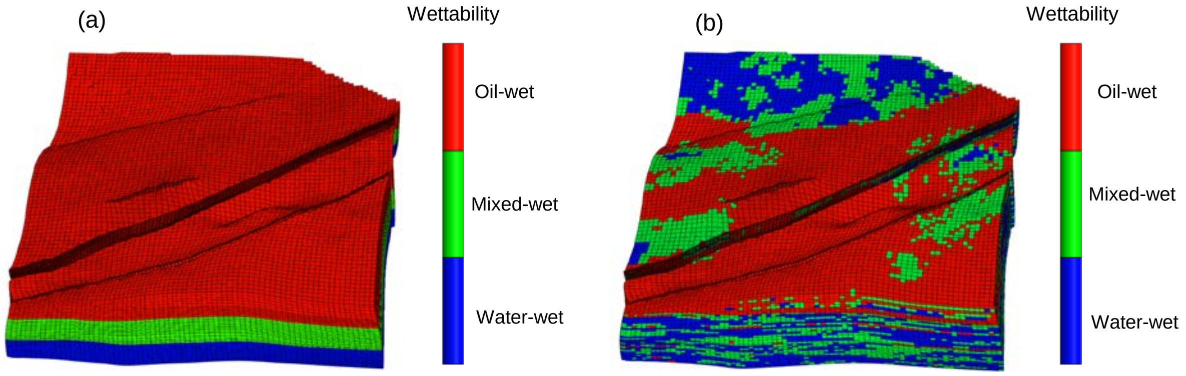

Fig. 6. Distribution of wettability in the simulation model using (a) depth based approach (DBA) and (b) facies based approach (FBA). DBA distributes wettability based on variation with depth while FBA correlates wettability to the horizontal permeability of individual grid blocks based on the facies type.

2.3 Fracture-Matrix Interaction

The special nature of fractured reservoirs lies in the interaction between the low permeability matrix which provides the main storage in the reservoir and the high permeability fracture system which has low storage. This combination of low-permeability matrix and high-permeability fractures leads to variety of flow behaviours in fractured carbonate reservoirs, including permeability enhancement, flow anisotropy, structurally induced bypassing of oil and rapid water/CO_2 breakthrough. These behaviours must be understood to adequately predict long-term reservoir behaviour. Therefore, special care is required to capture the geological complexity of fracture systems in a form that can be represented in reservoir models. Discrete fracture network (DFN) models are commonly used to generate static fracture models (Dershowitz et al., 2000). The models are then calibrated to dynamic data from well tests or production logging tests (e.g., Wei et al., 1998;

Hoffman & Narr, 2012) before they are upscaled to provide permeability distributions for the fracture network. In commercial reservoir simulators, the fracture system, modelled and upscaled using the DFN approach, is coupled to the matrix system using dual-continuum models (e.g., Bourbiaux et al., 2002; Casabianca et al., 2007).

The interaction between fracture and matrix depends on the matrix properties (e.g. porosity, permeability and wettability) and the fracture network geometry. The interaction also depends on the displacement mechanisms and physical processes. Fracture-matrix fluid transfer during water injection in a naturally fractured reservoir is controlled by viscous, gravitational, and capillary forces (e.g., Lu et al., 2008)). The rate of fracture-matrix fluid exchange can be modelled using a transfer function that depends on the matrix wettability, matrix permeability and fracture intensity (e.g., Lu et al., 2008; Abushaikha & Gosselin, 2008; Ramirez et al., 2009; Al-Kobaisi et al., 2009). Spontaneous imbibition, i.e. capillary forces, displace oil from the matrix due to the counter-current flow of water in water-wet rocks but this effect decreases with decreasing water-wetness (Morrow and Mason, 2001; Schmid & Geiger; 2012, 2013). During CO_2 injection, gravity drainage controls the transfer of CO_2 into the matrix and concurrently the transfer of oil from the matrix into the fracture due to fluid density differences. This transfer mechanism is particularly important for mixed- to oil-wet reservoirs such as carbonates because the gravitational head can overcome the capillary entry pressure for the displacing gas phase (Di Donato et al., 2007; Lu et al., 2008).

2.4 Fracture Network Modelling and Upscaling

The fracture system was modelled using the DFN approach (Dershowitz et al., 2000) and honours detailed geological observations in the outcrop. Shekhar et al. (2010) identified three major fracture sets (Table 2 & Fig. 7). The mean fracture length was 20 m, while the aspect ratio (length to height) was 4:1. Variation of the fracture length with respect to the mean was defined using an exponential distribution. Fracture apertures with a mean of 0.5 mm were used to estimate fracture permeabilities from the cubic law.

Although, the models honour static observations of the fracture orientation, it is difficult to adequately capture the connectivity of the fracture network. Hence, the uncertainty in fracture connectivity is investigated by varying the fracture network volumetric intensity (P32). As previously noted, we investigate three distinct fracture geometry scenarios. First, we investigate a pervasive regional fracture scenario where the stochastic fracture intensity is constant across the whole model and defined by intensity values which vary from a poorly-connected system to a well-connected system (Fig. 8). We also investigate a bedding related fracture scenario defined in relation to bed-bound (stratigraphically confined) and interbedded fractures (Fig. 9). Finally, we investigate a fracture scenario where the fracture intensity is related to the fault zone. In this case, high fracture intensity close to the faults decreases away from the faults (Fig. 10). In our modelling we focus on open fractures and do not consider closed fractures that might have formed as a result of secondary mineralization. Vertical wells intersect fractures in all cases.

Table 2. Fracture sets used for stochastic fracture generation in all DFN models

	Type of distribution	Dip direction	Dip	Fracture length	Fracture aperture
		average	average	average	average
Set 1	Fisher	275	74	20 m	0.5 mm
Set 2	Fisher	315	75	20 m	0.5 mm
Set 3	Fisher	345	76	20 m	0.5 mm

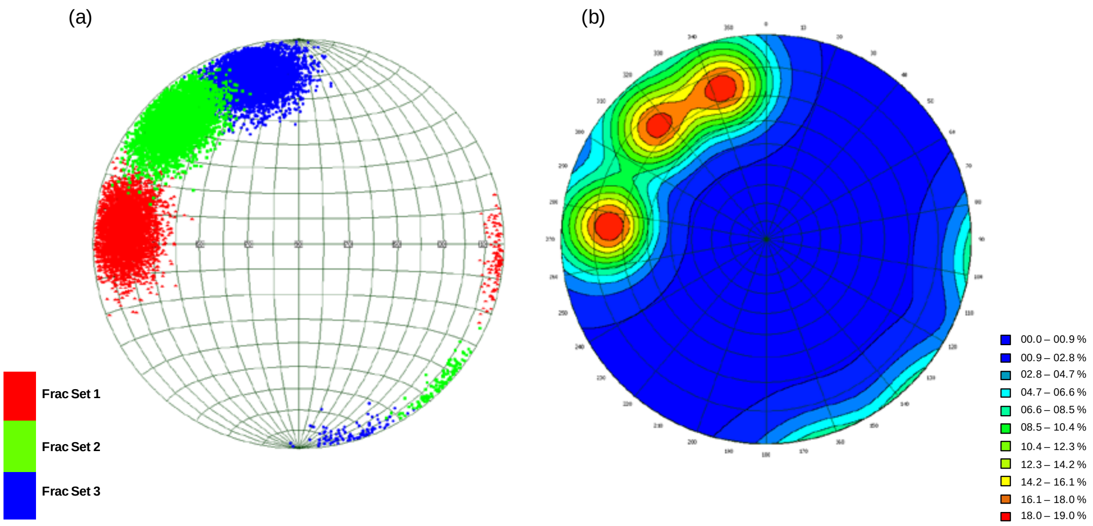

Fig. 7. Schmidt diagram showing the orientation distribution of three fracture-sets (red, green, blue) with equal projection of the poles in the upper hemisphere (a) and contoured density of fracture poles (b) based on fractures generated for the 3D reservoir model.

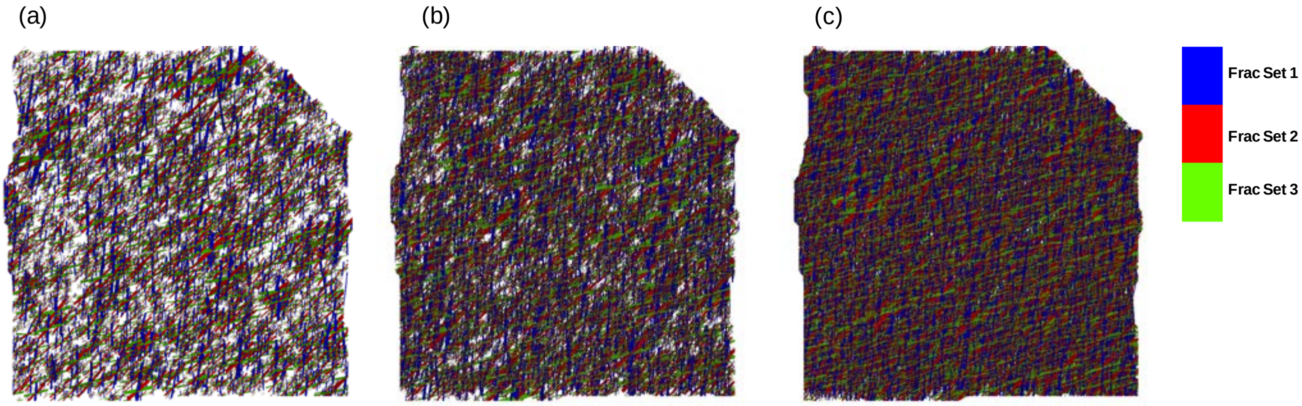

Fig. 8. Discrete fracture network for regional fracture scenario with fracture intensity of 0.05 m2/m3 (a), 0.1 m2/m3 (b) and 0.2 m2/m3 (c).

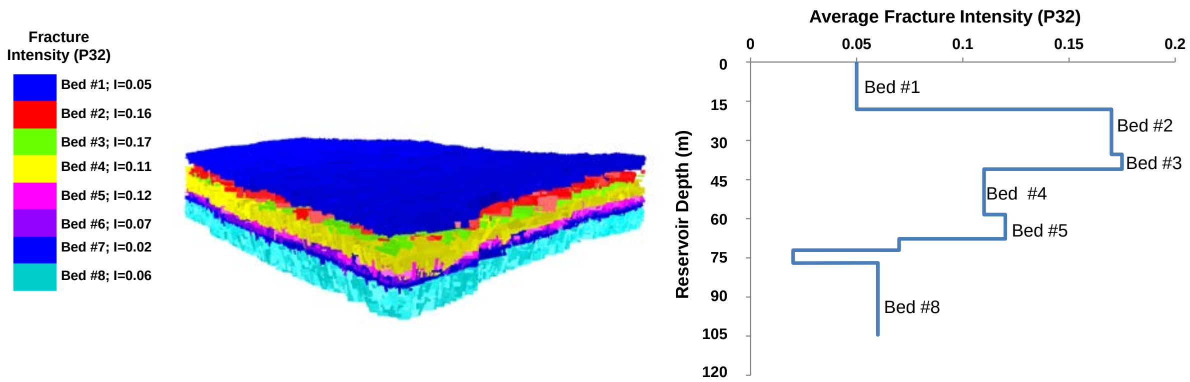

Fig. 9. Discrete fracture network for bedding related fracture scenario. 70% of the fractures terminate within a single bed, while 30% of the fractures penetrate multiple beds. The average fracture intensity for the entire model is 0.1 m2/m3.

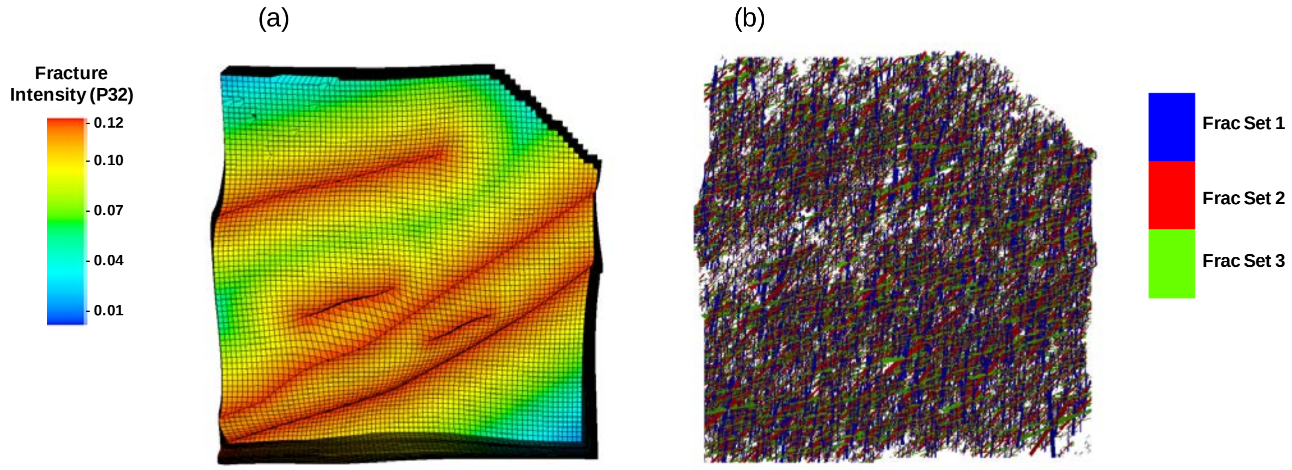

Fig. 10. Fracture intensity property (a) and discrete fracture network (b) for fault-related fracture scenario. The average fracture intensity for the entire model is 0.1 m2/m3.

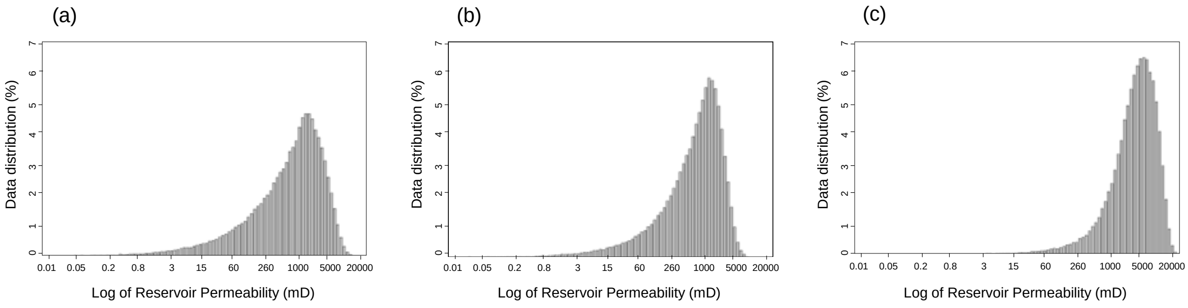

Fig. 11. Fracture permeability histogram for (a) regional, (b) fault related and (c) bedding related fracture scenarios. Note that fracture permeability assigned to the reservoir model grid blocks is on average about ten times higher than matrix permeability (see figure 4).

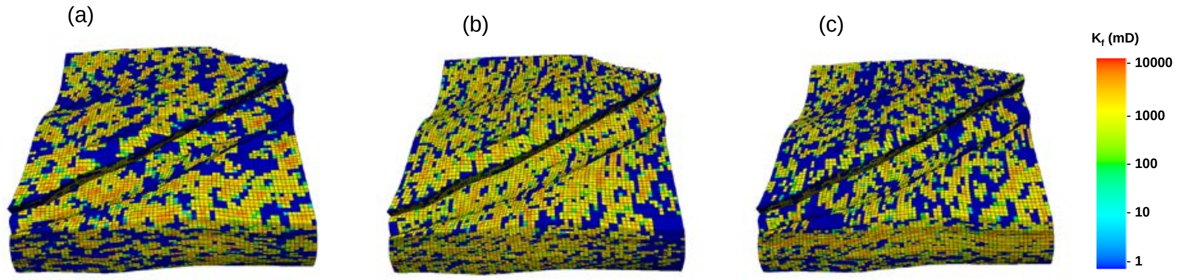

Fig. 12. Upscaled fracture permeability distribution for (a) regional, (b) fault related and (c) bedding related fracture scenarios. Average fracture intensity is 0.1 m2/m3 for all cases. Note high fracture permeability around faults in (b) and high fracture permeability layers due to stratigraphically confined fractures in (c).

Fracture network flow parameters for each DFN were obtained by upscaling the fracture networks to the grid cells of the simulation model (Fig. 11 & 12). We have chosen to use the modified Oda (1985) DFN upscaling method that is more computationally efficient than flow-based DFN upscaling and accurate for fracture systems with good connectivity. DFN upscaling, results in diagonal fracture permeability tensors that are anisotropic and heterogeneous and honour outcrop observations reasonably well.

We tested the use of linear (and non-linear) two-phase relative permeability curves to account for multiphase flow in the fractures but the simulation results were identical due to the small volume and the high permeability of the fractures. In such cases, intermediate saturations do not occur and the flow is not determined by the specific shape of the relative permeabilities. Hence, it was sufficient to use linear relative permeabilities in this study. If smaller fracture apertures and consequently lower fracture permeabilities are encountered, the intermediate saturations may have a greater influence on the simulation results and it is expected that non-linear curves would be employed.

Due to the, in parts, relatively high permeability in the matrix, a dual-porosity dual-permeability model was used to couple fluid flow in the matrix with fluid flow in the fractures and simulate multiphase flow for the range of plausible geological scenarios. It is well known that the dual permeability formulation is preferable in situations where there is hydraulic continuity in the matrix and high variability in the connectivity of the fracture network (Kazemi et al., 1992; Bourbiaux, 2002).

For a single-phase, dual-porosity dual-permeability model, flow in the matrix is given by:

$$\nabla \cdot \left(\frac{k_m}{\mu} \nabla p_m\right) - \frac{\sigma k_m}{\mu}\left(p_f - p_m\right) + q_m = \phi_m c_{tm} \frac{\partial p_m}{\partial t} \ , \tag{14}$$

while flow in the fractures (with an additional term for matrix flow contribution) is given by:

$$\nabla \cdot \left(\frac{k_f}{\mu} \nabla p_f\right) - \frac{\sigma k_m}{\mu}\left(p_f - p_m\right) + q_f = \phi_f c_{tf} \frac{\partial p_f}{\partial t} \ , \tag{15}$$

where, $k_f, p_f, q_f, \phi_f, c_{tf}$ and $k_m, p_m, q_m, \phi_m, c_{tm}$ represent the fracture and matrix permeability, pressure, source/sink, porosity and total compressibility respectively. μ is the fluid viscosity and σ is the shape factor which describes the area of fracture-matrix interface in each grid block. σ is obtained directly from DFN upscaling.

We used the Gilman and Kazemi (1983) transfer function to model the fluid exchange between fracture and matrix. The transfer function is a conservation of momentum formulation that takes oil expansion, capillary imbibition and gravity drainage recovery mechanisms into account. The transfer function follows the classic Warren-Root (1963) assumption that the flow towards the well bore takes place in the fracture network while the matrix feeds the system with stored hydrocarbons. Equations (16) and (17) describe the Gilman and Kazemi formulation for the transfer of oil and water between fracture and matrix domains.

$$T_o = \sigma \frac{k_m k_{ro}}{\mu_o}\left(p_o^m - p_o^f + (\rho_w - \rho_o)\left(S_{wD}^f - S_{wD}^m\right)\frac{gh}{2}\right) \quad (16)$$

$$T_w = \sigma \frac{k_m k_{rw}}{\mu_w}\left(p_o^m - pc_o^m - p_o^f + pc_o^f + (\rho_w - \rho_o)\left(S_{wD}^f - S_{wD}^m\right)\frac{gh}{2}\right) \quad (17)$$

where T_o represents the transfer of oil from the matrix to the fractures and T_w represents the transfer of water from the fractures to the matrix in the case of capillary imbibition. $k_{ro}\ and\ k_{rw}$ are the oil and water relative permeabilities, respectively. g is the gravity term while h is the height of the matrix blocks. $\rho_o,\ \rho_w$ represent the oil/water density and S_{wD} is the dimensionless water saturation. We also tested the Quandalle and Sabathier (1989) transfer function which is known to capture gravitational flow more accurately but found the results to be identical.

The resulting reservoir models, containing fractures and matrix, are populated with the same fault network, mapped using high-resolution photopanels and LiDAR (Light Detection And Ranging). The faults are represented as discrete non-volumetric features in the geological model. In general, we consider the faults to be fully conductive, with flow reduction across faults occurring only due to the juxtaposition of high and low permeability layers. More detailed fault models are not within the scope of this study.

3. Results

3.1 Effect of fracture network intensity

Figure 13 shows upscaled fracture permeabilities and the corresponding matrix saturation distributions for the DFN models assuming P32 of 0.05 m^2/m^3, 0.1 m^2/m^3, 0.2 m^2/m^3 and 0.4 m^2/m^3 (a, b, c and d). The oil saturation distributions (e, f, g and h) and CO_2 saturation distributions (i, j, k and l), show a clear link between the fracture intensity and the predicted oil and CO_2 distributions. As the fracture intensity increases, there is more rapid transport of injected water and CO_2 leading to significant bypassing of oil in the matrix. Similarly, as the fracture intensity increases, rapid transport of CO_2 leads to high CO_2 concentration at the top of the reservoir. Such rapid gas transport will lead to less efficient CO_2 sequestration in the matrix. As noted before, capillary imbibition and gravity drainage are important oil recovery and CO_2 storage mechanisms for fractured reservoirs. These mechanisms depend on exchange of fluids between the fracture and the matrix. However, if the flow in the fractures is rapid due to a well-connected fracture network, the residence time of injected fluids in the fracture becomes insufficient to adequately recover oil or store CO_2 in the matrix via spontaneous imbibition and gravity drainage, thereby leading to poor hydrocarbon recovery and CO_2 sequestration.

The influence of the fracture network can also be observed in the oil recovery, water cut and CO_2 storage profiles (Fig. 14). Notice that the presence of open and connected fractures in the reservoir results in lower oil recoveries (Fig. 14a), early water breakthrough (Fig. 14b), and lower fractions of CO_2 stored (Fig. 14c). The bypassing effect that leads to lower oil recovery increases as fracture intensity increases but becomes less significant at higher fracture intensities (P32 >= 0.4). This behaviour may suggest that in systems where the fracture network is very dense, above a certain threshold, variations in model output due to changes to the fracture network could be negligible thereby potentially reducing the impact of the fracture uncertainty on the model outcomes.

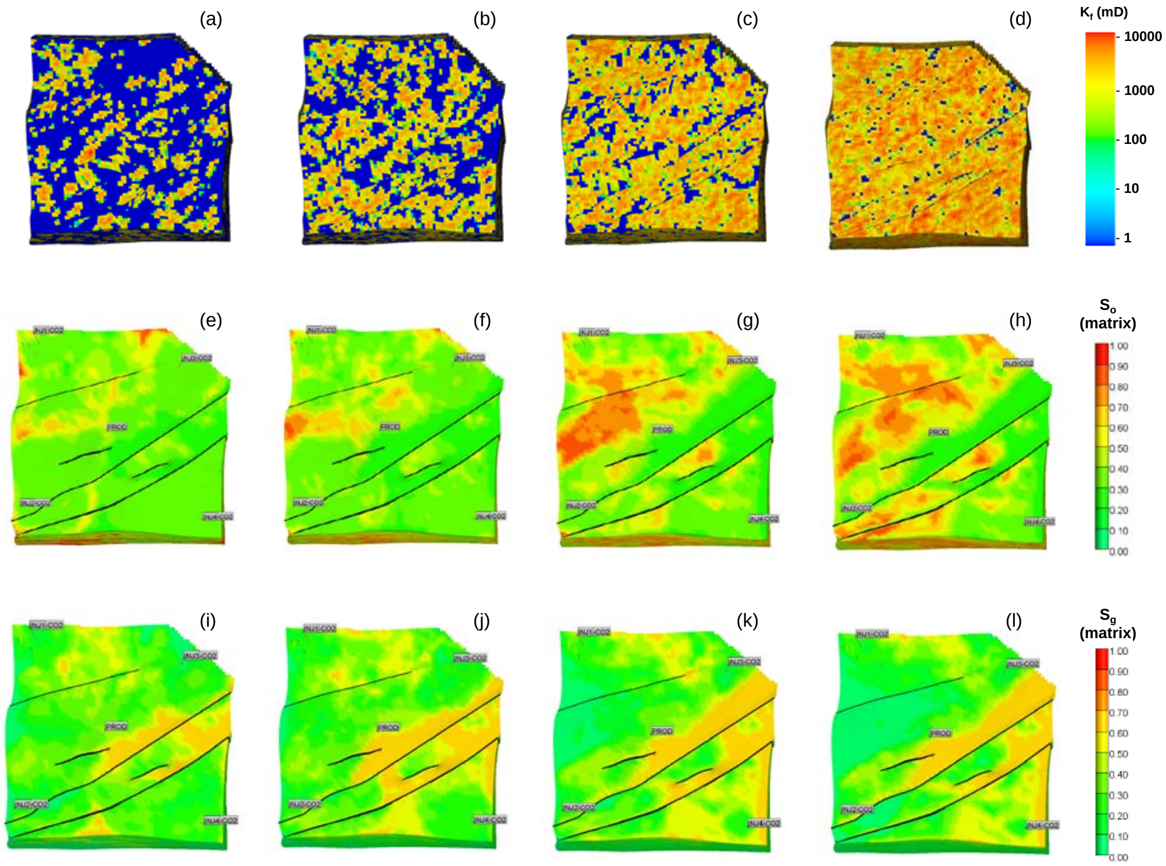

Fig. 13. Upscaled fracture permeability distribution with increasing regional fracture intensity of 0.05 (a) 0.1 (b) 0.2 (c) 0.4 (d) and corresponding matrix oil saturation (e, f, g, h) and CO_2 saturation (i, j, k, l) distributions after immiscible WAG injection. Notice the bypassed oil and high CO_2 concentration at the top of the model due to rapid flow of reservoir fluids.

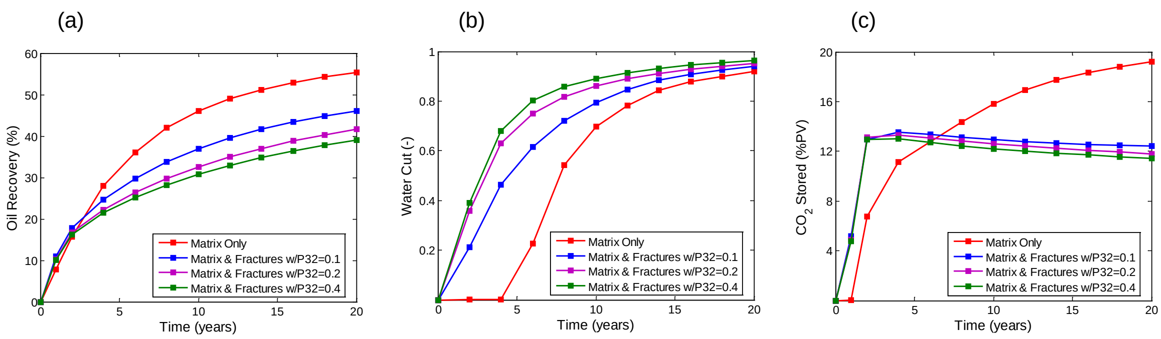

Fig. 14. Oil recovery (a), water cut (b) and CO_2 stored (c) during immiscible WAG injection. Fractures are incorporated with dual-porosity dual-permeability models of increasing fracture intensity (P32). Fracture networks cause bypassing and act as fluid flow high ways leading to lower oil recovery, early water breakthrough and lower fraction of CO_2 stored.

3.2 Effect of fracture network geometry

At low fracture network intensity (for example, P32 = 0.1), subtle conceptual changes in the static modelling of the fracture geometry, impact the simulation results more significantly than at higher fracture network intensity (for example, P32 = 0.5). We considered three fracture geometry scenarios; (1) Regional fracture geometry (2) Fault related fracture geometry and (3) Bedding related fracture geometry. For an average fracture network intensity of 0.1, the oil recovery varies between 45%, 43% and 42%, assuming regional, fault related or bedding related fracture geometry respectively (Fig. 15a, b, c and Fig. 16a). Conversely, the oil recovery profiles are indistinguishable when the fracture network intensity is 0.5, irrespective of the specific fracture network geometry (Fig. 16d). The results indicate that the fracture intensity is a controlling parameter: Above a given fracture intensity, simulation results are largely independent on the underlying geological concept that was used to model the fracture network. Below this threshold fracture intensity, simulation results depend on the geological concepts that underpin the fracture model.

Similarly, the water cut varies between 96%, 95% and 94% (Fig. 16b), while the CO_2 stored varies between 12%, 13% and 14% of the pore volume assuming bedding related, fault related or regional fracture geometry respectively (Fig. 15d, e, f and Fig. 16c). The bedding related fracture system contains layer-oriented fracture permeabilities that may lead to the prevalence of high permeability layers and exacerbate flow channelling, thereby yielding the lowest estimated oil recovery and CO_2 stored. As noted above, at high fracture intensity, the influence of the specific fracture geometry is less distinguishable because the fracture density is so high that fractures are fully connected and form long-range high-permeability flow paths irrespective of the specific geometry (Fig. 16d, e, f).

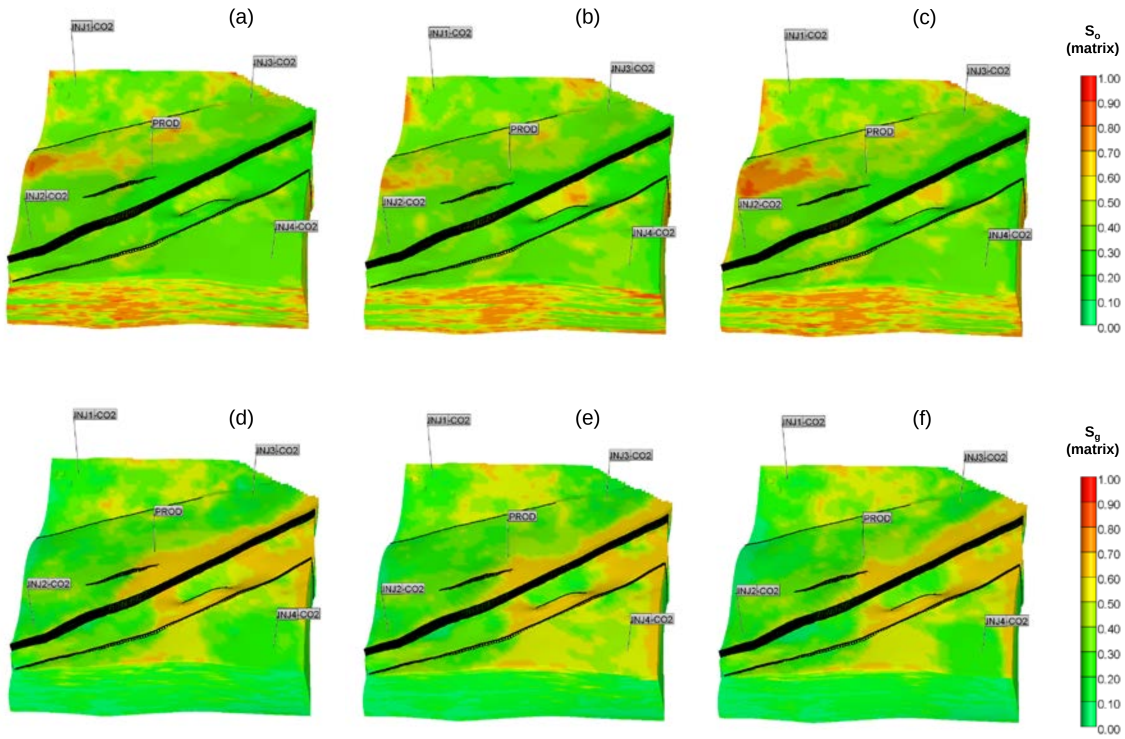

Fig. 15. Oil saturation (a, b, c) and CO_2 saturation (d, e, f) distribution during immiscible WAG injection in the fractured carbonate reservoir with regional (a, d), fault related (b, e), and bedding related (c, f) fracture geometries. The average fracture intensity is 0.1 m^2/m^3 in all cases.

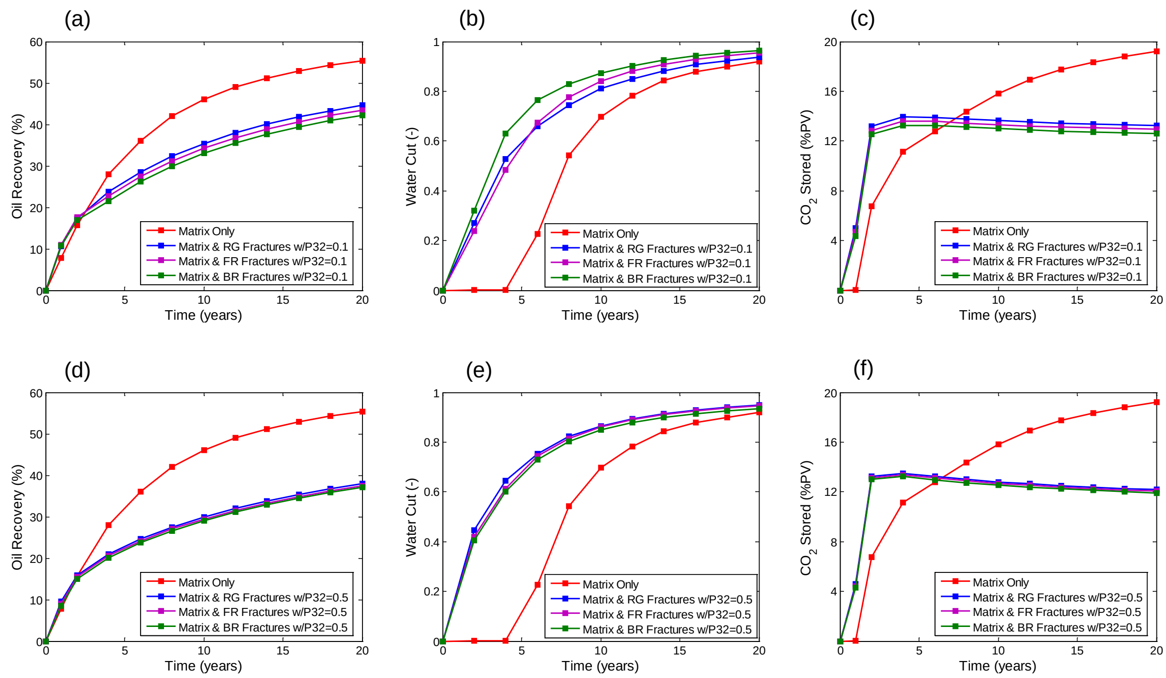

Fig. 16. Oil recovery (a, d), water cut (b, e) and CO_2 stored (c, f) when regional (RG), fault-related (FR) and bedding-related (BR) fracture geometry scenarios are considered. 'P32' refers to the "average fracture intensity". We assume that P32 = 0.1 m^2/m^3 indicates low fracture intensity while P32 = 0.5 m^2/m^3 indicates high fracture intensity. Oil recovery and CO_2 storage profiles are less distinguishable at high fracture intensities.

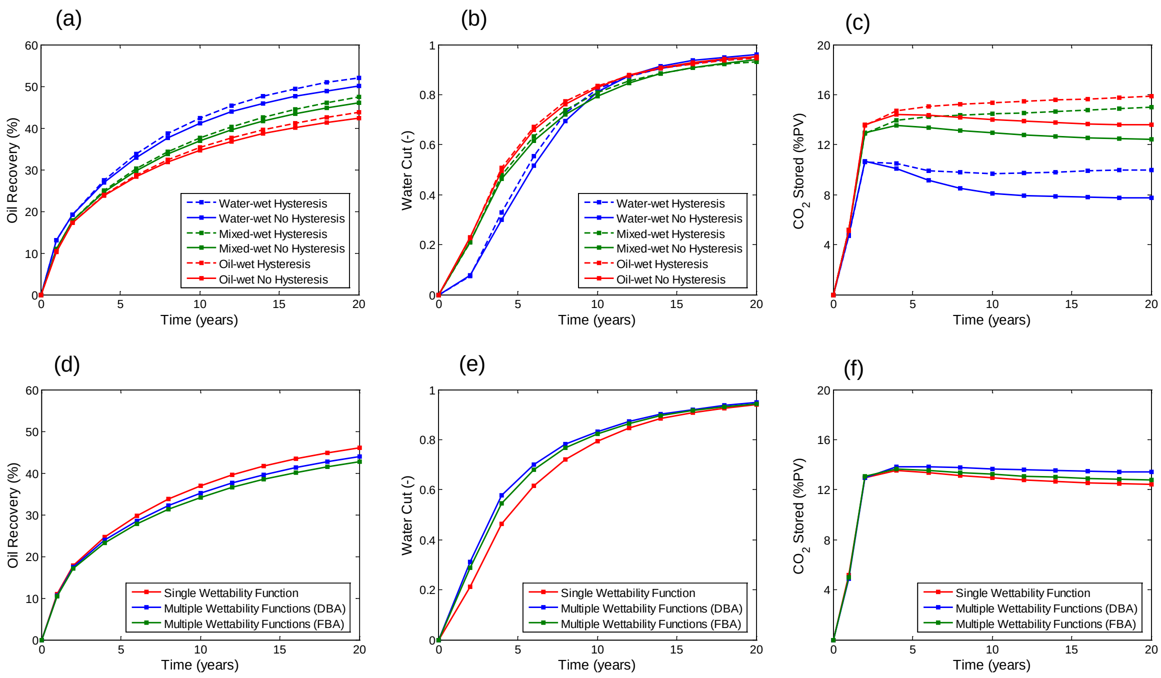

Fig. 17. Oil recovery (a, d), water cut (b, e) and CO_2 storage (c, f) profiles during immiscible WAG injection. Water-wetness improves imbibition, gives highest recovery fractions and results in slower water transport; however, lower volumes of CO_2 are stored under water-wet conditions due to high capillary entry pressure. DBA refers to a depth-based approach that correlates wettability to depth while FBA refers to a facies-based approach that correlates wettability to the horizontal permeability of the grid cells based on facies types.

3.3 Effect of matrix wettability

To ensure a tractable number of simulations while investigating important fluid flow effects, we have used the regional fracture scenario with average fracture intensity of 0.1 for all subsequent simulations. Unless otherwise stated, the base case for wettability in all simulations is the single mixed-wet wettability function. In general, higher oil recovery factors are encountered in all wettability scenarios when hysteresis is employed due to reduced mobility of the CO_2 phase and better oil displacement (Fig. 17a). When matrix wettability is varied in the flow simulations, it is observed that increasing water-wetness leads to higher oil recovery, which decreases under mixed-wet conditions and further decreases in oil-wet conditions (Fig. 17a). This is due to the high imbibition potential of water-wet formations (Morrow and Mason, 2001; Schmid and Geiger, 2012, 2013).

As previously noted, spontaneous imbibition is a major recovery mechanism in fractured reservoirs and a more water-wet rock will support efficient imbibition of water from the fractures to displace oil from the matrix through a counter-current or co-current mechanism. We can also compare the imbibition efficiency using the water cut profiles (Fig. 17b). We observe that the water cut increases more rapidly in the mixed-wet and oil-wet cases compared to the water-wet case due to the more efficient imbibition in the water-wet scenario. Conversely, the fraction of CO_2 stored is significantly lower in the water-wet case compared to the mixed-wet and oil-wet cases (Fig. 17c). The low CO_2 storage fraction in the water-wet case is due to the high capillary entry pressure of water-wet rocks that makes it difficult for CO_2 to be displaced into the matrix.

Furthermore, we test the impact of multiple approaches for distributing wettability in the model using saturation functions (see fig. 6). We include three scenarios; (1) Single mixed-wet saturation function for the entire reservoir, (2) Multiple saturation functions distributed using a depth based approach where the wettability varies from oil-wet at the top to water-wet at the bottom of the reservoir and (3) Multiple saturation functions distributed using a facies based approach where the wettability is assigned based on correlation to the horizontal permeabilities of the grid cells (Fig. 17 d, e, f).

When multiple saturation functions are employed, lower oil recovery but higher CO_2 storage fractions are observed. Since wettability controls imbibition and drainage mechanisms which in turn control oil recovery and CO_2 storage, such lower oil recoveries and higher CO_2 storage fractions are not surprising. In other words, the combined effect of the multiple saturation functions depends on how the end-members (oil-wet to water-wet) have been allocated to the grid cells based on the distribution approach. In this case the combined effect of the multiple saturation functions indicates that the oil recovery efficiency is less than for the scenario with a single mixed-wet wettability. The results demonstrate the uncertainties inherent to the wettability distribution method chosen and the importance of rigorous approaches for defining and distributing the saturation functions in simulation models for evaluating CO_2 EOR and storage (e.g., Gomes, 2008; Hollis et al., 2010; Chandra et al., 2015).

3.4 Effect of Hysteresis and Residual Trapping

To gain insight into the dynamic behaviour of the reservoir in cases with and without hysteresis, we identified three observation points in the simulation model and monitored the evolution of CO_2 saturation over 20 years (Fig. 18). Observation point #1 (grid cell 64, 67, 1) and observation point #2 (grid cell 57, 16, 1) are close to injection wells in the simulation model, while observation point #3 (grid cell 71, 30, 1) is located between two faults. Choosing the observation points in this way enabled us not only to observe the evolution of CO_2 saturation paths, but also to show the influence of geological features such as faults on trapping. We observe that the CO_2 saturation distribution at the top of the reservoir when hysteresis is not considered (Fig. 18a) is higher than the CO_2 saturation at the top of the reservoir when hysteresis is considered (Fig. 18b), indicating that the CO_2 plume migration to the top of the reservoir is much slower when hysteresis is considered and residual trapping is accounted for.

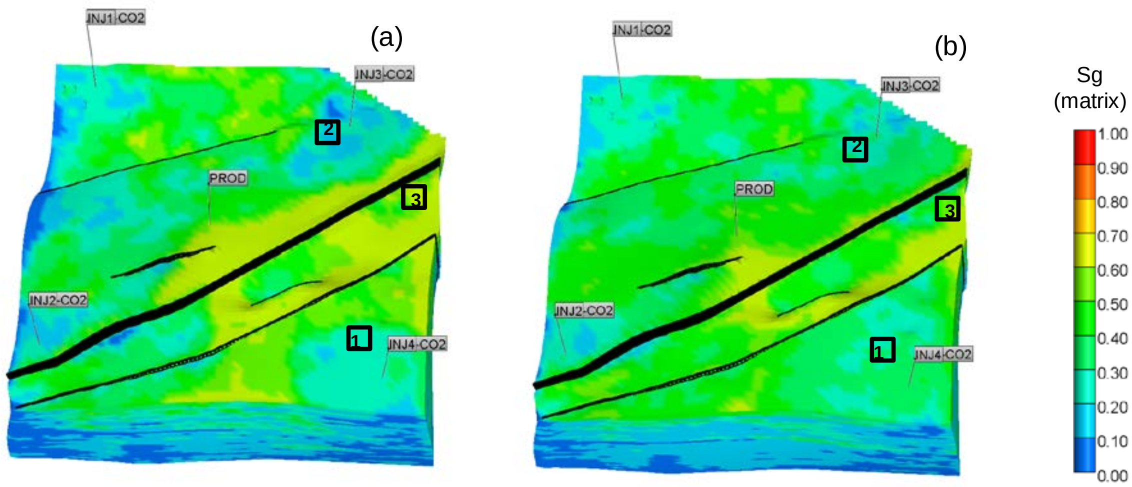

Fig. 18. Matrix gas saturation distribution during WAG injection without hysteresis (a) and with hysteresis (b). Three observation points (#1, #2, #3) are shown on the simulation model where CO_2 saturation is monitored over 20 years.

When hysteresis is considered, the model predicts a trail of residual, immobile CO_2 during the migration of the plume that reduces the overall mobility of CO_2 and leads to a more conservative estimate of the CO_2 distribution at the top of the reservoir (e.g., Juanes et al., 2006; Spiteri et al., 2006; Qi et al., 2008, 2009; MacMinn et al., 2011). Lower CO_2 distribution at the reservoir top is favourable for CO_2 sequestration because it reduces the potential of the gas to damage the cap rock and generate fissures in the cap rock which may then be conduits for CO_2 leakage to upper formations and ultimately to the atmosphere.

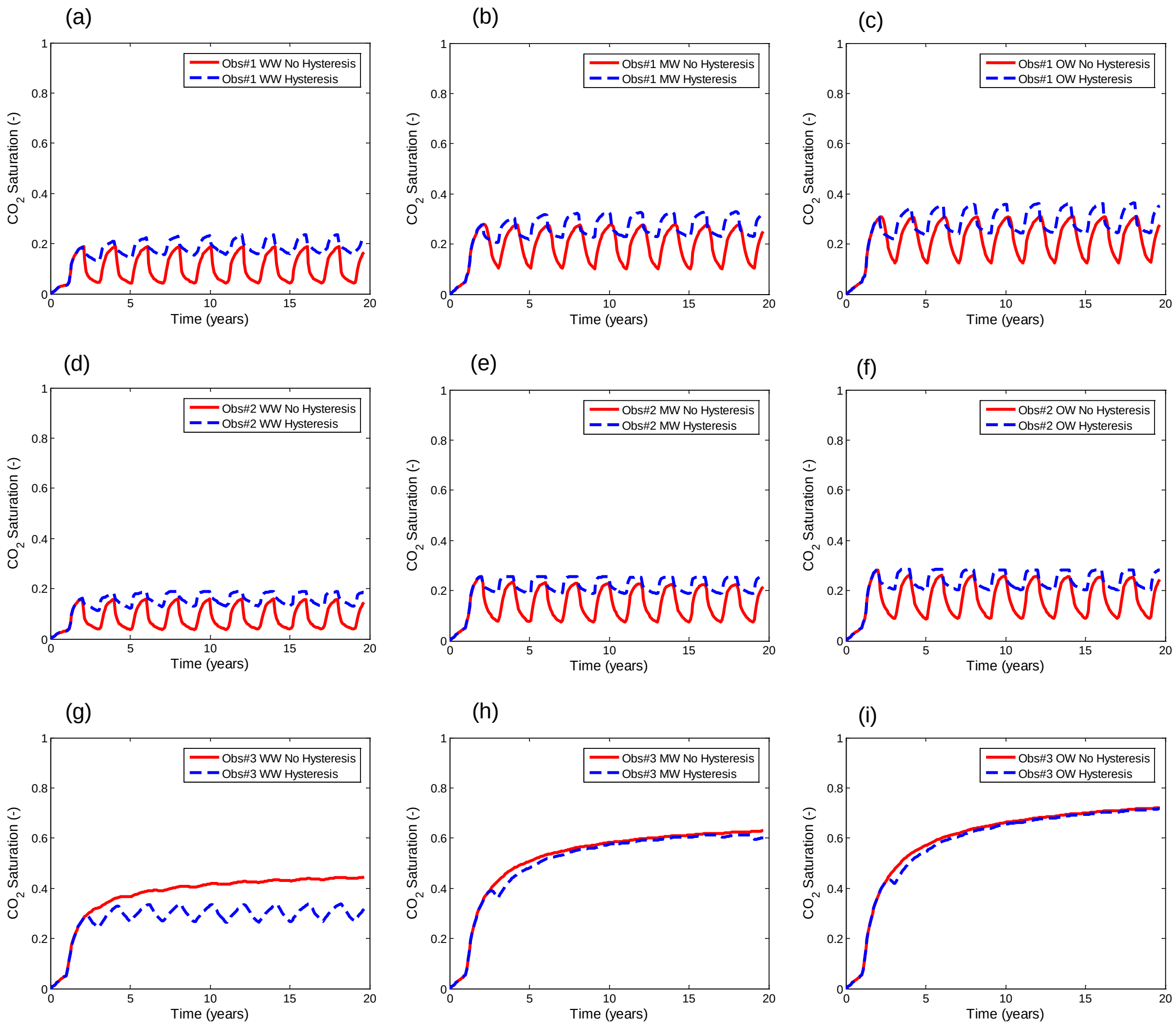

Fig. 19. Gas saturation profiles at observation points #1, #2, #3 (Fig. 18) under water-wet (a, d, g), mixed-wet (b, e, h) and oil-wet (c, f, i) conditions respectively. Water and CO_2 are injected during alternate cycles at equivalent rates of 1589 m^3/day.

Figure 19 shows CO_2 saturation evolution at the three observation points during WAG injection under water-wet, mixed-wet and oil-wet conditions. All the observation points indicate that the difference in CO_2 saturation profiles between the models with and without hysteresis begins in the third injection cycle. In the third injection cycle (W-G-W-G), water is injected into the reservoir after a flow reversal. If hysteresis is considered, water injection after flow reversal instigates residual CO_2 immobilisation and trapping, hence, the decrease in gas saturation follows a different evolution path compared to the model where hysteresis is not considered. Residual trapping hence reduces overall gas mobility, increases the stored gas fraction and improves oil recovery.

On average, the CO_2 saturation in the matrix of the water-wet models (Fig. 19a, d, g) is approximately 39% less than the CO_2 saturation in the matrix of the mixed-wet models (Fig. 19b, e, h) and 56% less than the CO_2 saturation in the matrix of the oil-wet models (Fig. 19c, f, i). The difference in matrix CO_2 saturation can be attributed to the high capillary entry pressure in water-wet rocks which supports spontaneous imbibition but opposes gas-oil gravity drainage. Hence, water-wet rocks exhibit high oil recovery during imbibition but low CO_2 storage during gas-oil gravity drainage. Conversely, oil-wet rocks exhibit low oil recovery during spontaneous imbibition but higher CO_2 storage during gas-oil gravity drainage.

At observation point #3, the behaviour of the gas saturation profiles differs from the other two observation points for all the wettability scenarios (Fig. 19g, h, i). This is due its location between two faults. We consider the faults to be fully conductive, with flow reduction across faults occurring only due to the juxtaposition of high and low permeability layers. Hence, only a small fraction of injected fluids reach observation point #3 due to viscous displacement. Consequently, hysteresis and residual CO_2 trapping (due repeat imbibition and drainage cycles) is limited and only observed in the water-wet scenario (due to the relatively stronger imbibition). The mixed-wet and oil-wet cases do not show hysteresis effects. The evolution of CO_2 saturation at the observation points therefore highlights the interaction and competition between recovery/sequestration mechanisms (e.g. gravity, capillary, viscous forces) and geological heterogeneity during CO_2 EOR and storage which needs to be captured in simulation models as we have done in this study.

3.5 Effect of WAG ratio and maximum trapped CO_2 saturation

We now investigate the effect of the WAG ratio and maximum trapped CO_2 saturation on the performance of CO_2 EOR and storage. The motivation is to consider what other factors influence the optimization of CO_2 sequestration during EOR. Specifically, to determine what factors can mitigate the influence of geological uncertainties and enable us to obtain the optimum displacement strategy for a specific reservoir (e.g., Wildenschild et al., 2011;

Doster et al., 2013). We observe that when the WAG ratio varies between 1:2, 1:1, 2:1 and 4:1, the total CO_2 stored (as a percentage of the reservoir pore volume) varies between 15%, 14%, 12% and 11% respectively (Fig. 20a). This is to be expected because as the WAG ratio increases a smaller fraction of CO_2 is injected into and subsequently stored in the reservoir. More importantly, figure 20a indicates that the WAG ratio can be varied to maximize CO_2 sequestration while producing oil within economic limits. The challenge, however, is that maximizing CO_2 sequestration simultaneously competes with maximizing the oil production (Fig. 20c). Obtaining an optimal economic solution for CO_2 EOR and storage is therefore nontrivial and may require the use of advanced optimization workflows to obtain the best solution while varying the model input parameters (e.g., Queipo et al., 2005; Oladyshkin et al., 2011; Koziel and Yang, 2011; Petvipusit et al., 2014).

Similarly, we observe that if the maximum trapped CO_2 saturation varies between 0, 0.2 and 0.4, for example, due to variations in wettability, injection rates and/or the injection strategy, the total CO_2 pore volume stored varies between 13%, 15% and 16% respectively (Fig. 21b) indicating a direct link between the maximum trapped saturation and the amount of CO_2 stored in the reservoir. Figure 20d demonstrates that improving the maximum trapped CO_2 saturation can increase the total amount of CO_2 stored in the reservoir with the total oil production remaining relatively constant. We can therefore use a better understanding of the mechanism of residual trapping to optimize CO_2 sequestration within economic limits.

We evaluate the effect of the WAG ratio and maximum trapped CO_2 saturation on the net gas utilization factor (GUF). The GUF indicates the amount of CO_2 that is stored in the reservoir for every barrel of oil produced (eqn. 18). The GUF is an important sequestration and economic parameter that quantifies the amount of CO_2 that can be safely stored in the reservoir during EOR.

$$GUF = \frac{CO_2\ Injected - CO_2\ Produced}{Oil\ Produced} \tag{18}$$

In general, higher volume of CO_2 is stored initially per barrel of oil produced (Fig. 20e, f). As the reservoir becomes gas saturated, the GUF reduces and becomes nearly constant. Figure

21e indicates that as the WAG ratio increases the GUF decreases. This is because higher WAG ratios produce larger quantities of oil at the expense of lower CO_2 storage (Fig. 20c).

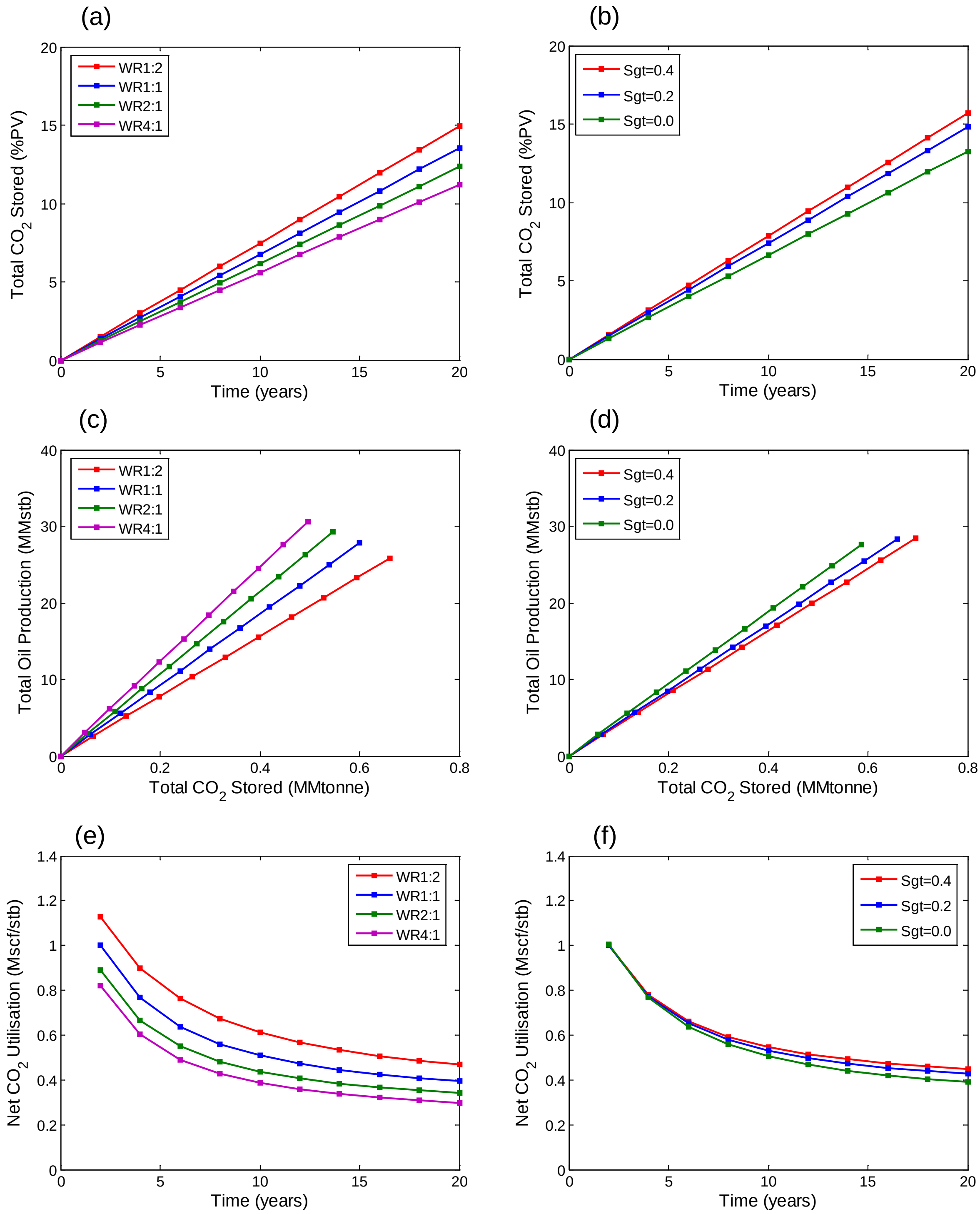

Fig. 20. Total CO_2 stored in the reservoir when WAG ratio (a, c) and maximum trapped gas saturation (b, d) are varied. As expected, larger volume of CO_2 is stored with low WAG ratios or high trapped saturations. The net CO_2 utilisation is higher at low WAG ratios (e) and increasing maximum trapped CO_2 saturation (f). All simulations consider the mixed-wet wettability scenario.

Finally, figure 20f demonstrates the impact of residual trapping on the net GUF. We see that as the trapped gas fraction increases, the net GUF increases indicating that a higher fraction of CO_2 is stored in the reservoir. This direct correlation between the trapped gas fraction and the net GUF, further reaffirms the fact that a better understanding of the mechanism of trapping can be used to optimize CO_2 sequestration (during EOR) within economic limits.

4. Discussion

Reservoir simulation is an important tool for investigating the fundamental controls on fluid flow in subsurface reservoirs during CO_2 EOR and storage (e.g., Jessen et al., 2005; Qi et al., 2009; Jenkins et al., 2012; Wriedt et al., 2014). Results from reservoir simulation can be used to evaluate the reservoir's suitability for CO_2 EOR and storage based on the influence of uncertain physical and geological parameters. Our simulation study shows that the fracture properties are a first order control on oil recovery and CO_2 storage efficiency in fractured carbonate reservoirs (Fig. 21). We find significant variations in subsurface flow behaviour when low intensity fractures are encountered compared to high intensity fractures, thereby, highlighting geological tipping points that influence simulation predictions. Hence, accurate characterisation and calibration of the hydrodynamic properties of the fracture network is essential. Calibrating simulation results based on static data with dynamic information from pressure transient, tracer and field tests can increase our understanding of a dynamically coupled fracture-matrix system. However, it should be noted that the complex interaction of fracture-matrix flow in fractured carbonate reservoirs can render the calibration of fractured carbonate reservoir models with pressure transient data difficult (Wei et al., 1998; Corbett et al., 2012; Agada et al., 2014).

We have also shown that the choice and number of saturation functions used to represent the wettability distribution can influence oil recovery and CO_2 storage predictions in fractured carbonates. It has been shown previously that accurate distribution of wettability for carbonates is a crucial aspect of carbonate reservoir characterization (e.g., Lichaa et al., 1993; Jerauld and Rathmell, 1997; Hollis et al., 2010; Chandra et al., 2015). In particular, using a single saturation function based on the assumption of uniform reservoir wettability is insufficient and the distribution of multiple saturation functions to reflect heterogeneous wettability offers more robust results. Relative permeability hysteresis also has a significant impact on subsurface CO_2 EOR and storage, as we have demonstrated. Modelling hysteresis in detail will account for the residually trapped (immobilised) CO_2 fraction and lead to reduction of the overall CO_2 phase mobility. Hence, understanding the mechanism of residual trapping means that trapping may be optimized to obtain significant economic and environmental benefit (e.g., Wildenschild et al., 2011; Doster et al., 2013).

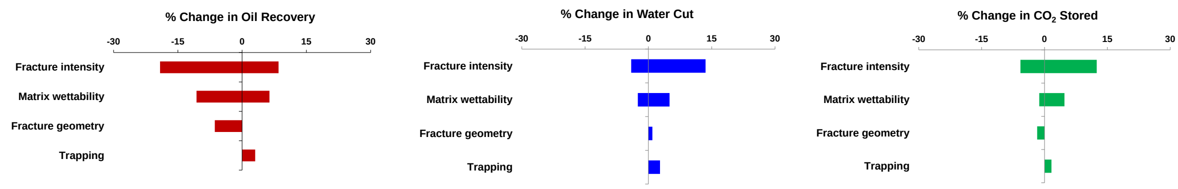

Fig. 21. Summary of the sensitivities affecting CO_2 EOR & Storage. Tornado chart shows the difference in the simulation results when individual parameters are varied between their minimum and maximum values. The base case for comparison is a regular five-spot pattern for WAG injection in the matrix coupled with regional fractures. The matrix wettability for the base case is "mixed-wet" while the average fracture intensity is 0.1. Hysteresis is not accounted for in the base case.

For all the sensitivities investigated, we used a traditional sensitivity analysis carried out by varying "one parameter at a time" to show that the fracture intensity, matrix wettability, fracture geometry and residual trapping are key uncertainties for CO_2 EOR and storage prediction (Fig. 21). This kind of sensitivity analysis, though very useful, could be biased because it may not fully explore the parameter space. Firstly, the tornado chart is based on the maximum and minimum parameter values considered in this study, but the end-members could differ if other scenarios are considered for given parameters (e.g., the conceptual fracture network geometry). Secondly, traditional sensitivity analysis assumes that the varied parameters are independent of each other, although in reality the parameters are often correlated. For example, matrix wettability and fracture intensity may have an interrelated rather than independent impact when controlling imbibition, drainage and residual trapping mechanisms. Recently, design of experiments (DoE) has been increasingly used as a means to set up multiple numerical simulations that maximize the amount of information acquired from a limited number of simulation runs. DoE provides a structured way to change multiple settings in order to understand the impact of the most influential and interrelated factors on CO_2 EOR and storage. Furthermore, DoE can be coupled with advanced optimization workflows to optimise and improve the economics of oil recovery and the CO_2 sequestration in fractured carbonate reservoirs (Friedmann et al., 2003; Koziel & Yang, 2011; Li & Zhang, 2014).

We coupled the fracture network with the rock matrix using traditional DFN modelling approaches and dual continuum formulations. Employing discrete fracture and matrix models (DFM) where the fractures are explicitly represented may provide additional insights into fracture-matrix transfer processes, especially in reservoirs where flow in the matrix is significant (e.g., Matthäi et al., 2007; Haegland et al., 2009; Geiger et al., 2009). Another source of uncertainty in the dual-continuum simulations is the shape factor (embedded in the transfer function) which for classical models (Warren and Root, 1963; Gilman and Kazemi, 1983) determines the speed of recovery from the matrix, but does not adequately capture the changes in recovery speed over time. This variability in recovery speed is due to sub-grid heterogeneities that are typical for fractured carbonate reservoirs and have been shown to significantly influence multiphase flow predictions. Hence, current research efforts are tailored towards generating novel multi-rate transfer functions that account for variable recovery speeds as a result of sub-grid heterogeneities (Di Donato et al., 2007; Geiger et al., 2013; Maier et al., 2013).

A regular five-spot well pattern was chosen as the standard well placement option for all the simulations in this study. It is important to note that the chosen well placement was not final and the oil recovery and CO_2 sequestration estimates may be improved by exploring different well placement approaches. More common well placement options that may have an impact on the simulation results include inverted five-spot, direct line drive and staggered line drive well patterns. Alternatively, robust well-pattern optimization which is now a standard technique in reservoir simulation may be employed to maximize CO_2 EOR and storage for a given well placement option while accounting for geological uncertainty with multiple model realisations (e.g., Bangerth et al., 2006; Oladyshkin et al., 2011; Onwunalu & Durlofsky, 2011; Petvipusit et al., 2014).

Since this study focused on short term CO_2 EOR and storage (only 20 years), we assumed that black oil simulation was sufficient to capture the short term effects of hysteresis, wettability and fracture-matrix interaction. Longer term CO_2 EOR and storage studies (approx. 100 – 1000 years) that need to capture complex flow processes such as CO_2 solubility and geochemical CO_2-rock interactions would benefit greatly from applying compositional simulations. The challenge remains that field-scale simulation of fractured carbonate reservoirs is very time consuming. Hence, it is worthwhile to investigate non-reactive CO_2 behaviour using black oil simulations prior to investigating reactive and multicomponent CO_2 behaviour using compositional simulation (e.g., Jessen et al., 2005).

5. Conclusion

The main objective of this paper was to investigate how the interplay between hysteresis, wettability and fracture-matrix exchange impacts oil recovery and CO_2 sequestration in relation to the multiscale heterogeneities that are pervasive for fractured carbonate reservoirs. We have shown that the specific fracture network geometry has a direct effect on oil recovery and CO_2 storage, especially when the fracture intensity is low. When the fracture intensity is high, the impact of varying fracture network geometry on oil recovery and CO_2 storage becomes less distinguishable. This is because the fracture density is so high that fractures are highly connected and form long-range high-permeability flow paths irrespective of the specific geometry. Thus, the fracture network properties, specifically the fracture intensity, exhibit "tipping point" behaviour that significantly influence the simulation output depending on whether the fracture intensity is low or high. We demonstrate that for a given fracture geometry, the presence of connected fractures leads to increased bypassing of the oil in the matrix by the injected fluids as the fracture intensity increases. The presence of connected fractures also leads to rapid CO_2 transport, relatively poor CO_2 sequestration and early water breakthrough.

We find that although the fracture network properties have the greatest impact on the simulations, yet the effect of wettability on CO_2 EOR and storage cannot be neglected. Water-wet reservoir conditions lead to reduced gas saturation in the matrix due to high capillary entry pressures that oppose gas oil gravity drainage. Increased imbibition in the water-wet medium also leads to higher oil recovery during water injection cycles. Conversely, the imbibition potential is very poor in the oil-wet medium leading to much lower recovery from water injection cycles. Residual trapping of the CO_2 is more significant in water-wet rocks because snap-off occurs and gas becomes increasingly disconnected in the pore throats from the continuous CO_2 phase. Because residual trapping entails a reduction of the CO_2 mobility, it ultimately leads to higher oil recovery. Reducing the CO_2 mobility delays CO_2 breakthrough, increases the stability of gas-water mobility front and improves contact of CO_2 with residual oil, thereby ensuring better macroscopic and microscopic sweep of the reservoir while increasing the residually trapped CO_2 fraction.

Simulation of fractured carbonate reservoirs can provide valuable insights on the suitability of a given reservoir for CO_2 EOR and storage. Simulation studies can also highlight the principal physical and structural uncertainties that control oil recovery and CO_2 sequestration with a view to mitigating these uncertainties. Bypassing of oil in the matrix, rapid CO_2 migration and early water breakthrough, for example, which are due to high fracture-matrix connectivity can be reduced by increasing the viscosity of the injected fluid using polymer injection and foam flooding applications. The wetting preference of the reservoir rock may also be altered by the injection of chemicals (e.g. surfactants) to achieve maximum CO_2 EOR and storage. Hysteresis in cyclic floods must be accounted for to ensure that simulations provide robust results that can guide subsurface reservoir management. The trade-off between the volumes of CO_2 trapped and the amount of oil recovered must also be optimised in the light of economic constraints including the source and cost of CO_2 delivered to the operational site.

Acknowledgements

The authors would like to thank the ExxonMobil $(FC)^2$ Research Alliance for funding this project. Sebastian Geiger is grateful to Foundation CMG for supporting his chair in carbonate reservoir simulation. We acknowledge Computer Modelling Group, Schlumberger and Golder Associates for providing access to commercial software. The research presented in this paper has benefitted from technical collaboration and numerous discussions with members of the former ExxonMobil (FC)^2 Research Alliance.

References

Abushaikha, A. S. & Gosselin, O. R. 2008. Matrix-fracture transfer function in dual-medium flow simulation: review, comparison and validation. Paper SPE 113890, presented at SPE Europec Annual Conference and Exhibition, Rome, 9-12 June.

Agada, S., Chen, F., Geiger, S., Toigulova, G., Agar, S., Shekhar, R., ... & Immenhauser, A. 2014. Numerical simulation of fluid-flow processes in a 3D high-resolution carbonate reservoir analogue. *Petroleum Geoscience*, *20*(1), 125-142.

Agar, S. M. & Geiger, S. 2015. Fundamental controls on fluid flow in carbonates: current workflows to emerging technologies. In: Agar, S.M. & Geiger, S. (eds) *Fundamental Controls on Fluid Flow in Carbonates*. Geological Society, London, Special Publications, **406(1)**, 1-59.

Al-Dhahli, A., van Dijke, M. I., & Geiger, S. 2013. Accurate modelling of pore-scale films and layers for three-phase flow processes in clastic and carbonate rocks with arbitrary wettability. *Transport in porous media*, *98*(2), 259-286.

Al-Dhahli, A., Geiger, S., & van Dijke, M. I. 2014. Impact of pore-scale three-phase flow for arbitrary wettability on reservoir-scale oil recovery. *Journal of Petroleum Science and Engineering*, *121*, 110-121.

Al-Futaisi, A. & Patzek, T. W. 2003. Impact of wettability alteration on two-phase flow characteristics of sandstones: A quasi-static description, *Water Resources Research*, **39**, 1042, doi:10.1029/2002WR001366

Al-Kobaisi, M., Kazemi, H., Ramirez, B., Ozkan, E. & Atan, S. 2009. A critical review for proper use of water/oil/gas transfer functions in dual-porosity naturally fractured reservoirs: Part II. *SPE Res. Eval & Eng.***12** (2), 211-217.

Amour, F., Mutti, M., Christ, N., et al. 2013. Outcrop analogue for an oolitic carbonate ramp reservoir: A scale-dependent geologic modelling approach based on stratigraphic hierarchy. *AAPG Bulletin*, **97**, 845-871.

Awan, A. R., Teigland, R. & Kleppe, J. 2008. A survey of North Sea enhanced-oil-recovery projects initiated during the years 1975 to 2005. *SPE Reservoir Evaluation & Engineering*, **11**, 497-512.

Azzolina, N. A., Nakles, D. V., Gorecki, C. D., Peck, W. D., Ayash, S. C., Melzer, L. S., & Chatterjee, S. 2015. CO2 storage associated with CO2 enhanced oil recovery: A statistical analysis of historical operations. *International Journal of Greenhouse Gas Control*, *37*, 384-397.

Bachu, S., Gunter, W. D., & Perkins, E. H. (1994). Aquifer disposal of CO_2: Hydrodynamic and mineral trapping. *Energy Conversion and Management*, **35**(4), 269-279.

Baker, L. E. 1988. Three-phase relative permeability correlations. Paper SPE 17369 presented at the SPE Enhanced Oil Recovery Symposium, Tulsa, Oklahoma, 16-21 April.

Bangerth, W., Klie, H., Wheeler, M. F., Stoffa, P. L. & Sen, M. K. 2006. An optimization algorithm for the reservoir oil well placement problem. *Computational Geosciences*, **10**, 303–319.

Belayneh, M. & Cosgrove, J. W. 2010. Hybrid veins from the southern margin of the Bristol Channel Basin. *UK Journal of Structural Geology*, **32**, 192-201.

Benisch, K., & Bauer, S. 2013. Short-and long-term regional pressure build-up during CO_2 injection and its applicability for site monitoring. *International Journal of Greenhouse Gas Control*, *19*, 220-233.

Blunt, M. 1997. Effects of heterogeneity and wetting on relative permeability using pore level modeling. *SPE J*, ***2***(1), 70-87.

Blunt, M. J. 2000. An empirical model for three-phase relative permeability. *SPE Journal*, 5(4), 435-445.

Blunt, M. J., Jackson, M. D., Piri, M., & Valvatne, P. H. 2002. Detailed physics, predictive capabilities and macroscopic consequences for pore-network models of multiphase flow. *Advances in Water Resources*, *25*(8), 1069-1089.

Bourbiaux, B., Basquet, R., Cacas, M. C., Daniel, J. M., & Sarda, S. 2002. An integrated workflow to account for multi-scale fractures in reservoir simulation models: implementation and benefits. SPE 78489, In *Abu Dhabi International Petroleum Exhibition and Conference, 13-16, October.*

Burnside, N. M., & Naylor, M. 2014. Review and implications of relative permeability of CO2 brine systems and residual trapping of CO2. *International Journal of Greenhouse Gas Control*, **23**, 1-11.

Carlson, F. M. 1981. Simulation of relative permeability hysteresis to the nonwetting phase, Paper SPE 10157 presented at the SPE Annual Technical Conference and Exhibition, San Antonio, Texas, 5-7 October.

Casabianca, D., Jolly, R. J. H., & Pollard, R. 2007. The Machar Oil Field: waterflooding a fractured chalk reservoir. *Geological Society, London, Special Publications*, **270**(1), 171-191.

Chandra, V., Barnett, A., Corbett, P.W.M., Geiger, S., Wright, P., Steele, R., & Milroy, P. 2015. Effective integration of reservoir rock-typing and simulation using near-wellbore upscaling. *Marine and Petroleum Geology*, **67**, 307-326.

Chen, Z., Huan, G., & Ma, Y. (2006). *Computational methods for multiphase flows in porous media* (Vol. 2). Siam.

Christensen, J. R., Stenby, E. H. & Skauge, A. 2001. Review of WAG field experience. *SPE Res. Eval. & Eng.*, **4**, 97-106.

Clerke, E. A. 2009. Permeability, relative permeability, microscopic displacement efficiency, and pore geometry of M_1 bimodal pore systems in Arab D Limestone., *SPE Journal*, **14**(3), 524-531.

Corbett, P. W. M., Geiger, S., Valdez, M., Borges, C. & Garayev, L. 2012. The third porosity: understanding the role of hidden porosity in well test interpretation in carbonates. *Petroleum Geoscience*, **18**, 73–81.

Cosentino, L., Coury, Y., Daniel, J. M., et al. 2001. Integrated study of a fractured Middle East reservoir with stratiform super-k intervals – Part2: Upscaling and dual media simulation. Paper SPE 68184 presented at the Middle East Oil Show, Bahrain, 17-20 March.

Dake, L.P. 1998. *Fundamentals of Reservoir Engineering*. Elsevier.

Dernaika, M. R., Basioni, M. A., Dawoud, A., et al. 2013. Variations in bounding and scanning relative permeability curves with different carbonate rock types. *SPE Res. Eval. & Eng.*, **16**(3), 265-280.

Dershowitz, B., Lapointe, P., Eiben, T. & Wei, L. 2000. Integration of discrete feature network methods with conventional simulator approaches. *SPE Res. Eval. & Eng.*, **3**(2), 165 – 170.

Di Donato, G., Lu, H. Y., Tavassoli, Z. et al. 2007. Multi-rate transfer dual-porosity modeling of gravity drainage and imbibition. *SPE Journal*, **12**(1), 77-88.

Doster, F., Nordbotten, J. M., & Celia, M. A. 2013a. Impact of capillary hysteresis and trapping on vertically integrated models for CO_2 storage. *Advances in Water Resources*, **62**, 465-474.

Doster, F., Nordbotten, J. M., & Celia, M. A. 2013b. Hysteretic upscaled constitutive relationships for vertically integrated porous media flow. *Computing and Visualization in Science*, ***15***(4), 147-161.

Egermann, P., Vizika, O., Kallet, L., Requin, C. & Sonier, F. 2000. Hysteresis in three-phase flow: Experiments, modelling and reservoir simulations. Paper presented at the IEA workshop on enhanced oil recovery, Edinburgh, 20-22 September.

Ettehadtavakkol, A., Lake, L. W., & Bryant, S. L. 2014. CO_2-EOR and storage design optimization. *International Journal of Greenhouse Gas Control*, *25*, 79-92.

Ferno, M. A., Haugen, A. & Graue, A. 2011. Wettability effects on the matrix-fracture fluid transfer in fractured carbonate rocks. *Journal of Petroleum Science and Engineering*, **77**, 146-153.

Friedmann, F., Chawathe, A., & Larue, D. K. 2003. Assessing uncertainty in channelized reservoirs using experimental designs. *SPE Reservoir Evaluation & Engineering*, *6*(4), 264-274.

Gale, J. F. W., Laubach, S. E., Marret, R. A., et al. 2004. Predicting and characterizing fractures in dolostone reservoirs: using the link between diagenesis and fracturing. Geological Society, London, Special Publications, **235**, 177-192.

Geiger, S., Dentz, M., & Neuweiler, I. 2013. A Novel Multi-Rate Dual-Porosity Model for Improved Simulation of Fractured and Multiporosity Reservoirs. *SPE Journal*, **18**(4), 670-684.

Gilman, J. R., & Kazemi, H. 1983. Improvement of simulation of naturally fractured reservoirs. *SPE Journal*, **23**, 695-707.

Gomes, J. S., Ribeiro, M. T., Strohmenger, C. J., Negahban, S. & Kalam, M. Z. 2008. Carbonate reservoir rock typing – the link between geology and SCAL. Paper SPE 118284, presented at the Abu Dhabi International Petroleum Exhibition and Conference, Abu Dhabi, UAE, 3-6 November.

Guerreiro, L., Silva, A. C. & Alcobia V. 2000. Integrated reservoir characterisation of a fractured carbonate reservoir. Paper SPE 58995 presented at the SPE International Petroleum Conference and Exhibition, Mexico, 1-3 February.

Haegland, H., Assteerawatt, A., Dahle, H. K., Eigestad, G. T. & Helmig, R. 2009. Comparison of celland vertex-centered discretization methods for flow in a two-dimensional discrete-fracture–matrix system. *Advances in Water Resources*, **32**, 1740– 1755.

Hoffman, B. T., & Narr, W. (2012). Using production logs (PLT) to estimate the size of fracture networks. *Journal of Petroleum Science and Engineering*, *98*, 11-18.

Hollis, C., Vahrenkamp, V., Tull, S., Mookerjee, A., Taberner, C. & Huang, Y. 2010. Pore system characterization in heterogeneous carbonates: An alternative approach to widely-used rock-typing methodologies. *Marine and Petroleum Geology*, **27**, 772-793.

Hui, M. H., & Blunt, M. J. 2000. Effects of wettability on three-phase flow in porous media. *The Journal of Physical Chemistry B*, **104**(16), 3833-3845.

Iding, M. & Ringrose, P. 2010. Evaluating the impact of fractures on the performance of the In Salah CO2 storage site. *International Journal of Greenhouse Gas Control*, **4**, 242-248.

Jackson, M. D., Valvatne, P. H., & Blunt, M. J. 2003. Prediction of wettability variation and its impact on flow using pore-to reservoir-scale simulations. *Journal of Petroleum Science and Engineering*, *39*(3), 231-246

Jackson, M. D., Valvatne, P., H. and Blunt, M. J. 2005. Prediction of wettability variation within an oil/water transition zone and its impact on production. *SPE Journal*, **10**, 184-195.

Jadhunandan, P. P., & Morrow, N. R. (1995). Effect of Wettability on Waterflood Recovery for Crude-Oil/Brine/Rock Systems. SPE Res Eng 10 (1): 40–46.

Jenkins, C. R., Cook, P. J., Ennis-King, J., Undershultz, J., Boreham, C., Dance, T., ... & Urosevic, M. 2012. Safe storage and effective monitoring of CO_2 in depleted gas fields. *Proceedings of the National Academy of Sciences*,*109*(2), E35-E41.

Jerauld, G. R., & Rathmell, J. J. (1997). Wettability and relative permeability of Prudhoe Bay: a case study in mixed-wet reservoirs. *SPE Reservoir Engineering*, **12**(1), 58-65.

Jessen, K., Kovscek, A. R., & Orr, F. M. 2005. Increasing CO 2 storage in oil recovery. *Energy Conversion and Management*, *46*(2), 293-311.

Joekar-Niasar, V., Doster, F., Armstrong, R. T., Wildenschild, D., & Celia, M. A. 2013. Trapping and hysteresis in two-phase flow in porous media: A pore-network study. *Water Resources Research*, *49*(7), 4244-4256.

Joekar-Niasar, V., Hassanizadeh, S. M., & Leijnse, A. 2008. Insights into the relationships among capillary pressure, saturation, interfacial area and relative permeability using pore-network modeling. *Transport in Porous Media*, *74*(2), 201-219.

Juanes, R., Spiteri, E. J., Orr, F. M. & Blunt, M. J. 2006. Impact of relative permeability hysteresis on geological CO_2 storage. *Water Resources Research*, **42**(12), 1-13.

Kalam, Z., Al-Rawahi, A. S., Al-Hosani, I. A., Negahban, S. & Rehman, A. A. 2011. Miscible gas injection tests in Carbonates and its impact on field development. Paper SPE 148374 presented at SPE RCSC, Abu Dhabi, UAE, 9-11 Oct.

Kazemi, H., Gilman, J. R., & Elsharkawy, A. M. 1992. Analytical and Numerical Solution of Oil Recovery from Fractured Reservoirs with Empirical Transfer Functions. *SPE Reservoir Engineering*, ***7***(2), 219-227.

Killough, J.E., 1976. Reservoir simulation with history-dependent saturation functions. *SPE Journ*al, **16**, 37– 48.

Kovscek, A. R., Wong, H., & Radke, C. J. 1993. A pore-level scenario for the development of mixed wettability in oil reservoirs. *AIChE Journal*, *39*(6), 1072-1085.

Kovscek, A. R. 2002. Screening criteria for CO2 storage in oil reservoirs.*Petroleum Science and Technology*, *20*(7-8), 841-866.

Kovscek, A. R., & Cakici, M. D. 2005. Geologic storage of carbon dioxide and enhanced oil recovery. II. Cooptimization of storage and recovery. *Energy Conversion and Management*, *46*(11), 1941-1956.

Koziel, S., & Yang, X. S. 2011. *Computational optimization, methods and algorithms* (Vol. 356). Germany: Springer.

Land, 1968. Calculation of imbibition relative permeability for two- and three-phase flow from rock properties. SPEJ, Trans., AIME 243, 149-156.

Larsen, J. A. & Skauge, A. 1998. Methodology for numerical simulation with cycle-dependent relative permeabilities. *SPE Journal*, **3**, 163-173.

Leach, A., Mason, C. F., & Veld, K. V. T. 2011. Co-optimization of enhanced oil recovery and carbon sequestration. *Resource and energy Economics*, *33*(4), 893-912.

Lenhard, R. J. & Oostroom, M., 1998. A parametric model for predicting relative permeability-saturation-capillary pressure relationships of oil-water systems in porous media with mixed wettability. *Transport in Porous Media*, **31**,109-131.

Lenhard, R. J. & Parker, J. C. 1987. A model for hysteretic constitutive relations governing multiphase flow: 2. Permeability-saturation relations. *Water Resources Research*, **23**(12), 2197-2206.

Li, S. & Zhang, Y. 2014. Model complexity in carbon sequestration: a design of experiment and response surface uncertainty analysis. *International Journal of Greenhouse Gas Control*, **22**, 123-138.

Lichaa, P. M., Alpustun, H., Abdul, J. H., Nofal, W. A., & Fuseni, A. B. 1993. Wettability evaluation of a carbonate reservoir rock: *Advances in Core Evaluation III, Reservoir Management*, **327**.

Liu, H., Tellez, B. G., Atallah, T., & Barghouty, M. 2012. The role of CO_2 capture and storage in Saudi Arabia's energy future. *International Journal of Greenhouse Gas Control*, *11*, 163-171.

Lu, H. Y., Di Donato, G., & Blunt, M. J. 2008. General transfer functions for multiphase flow in fractured reservoirs. SPE *Journal*, **13**(3), 289-297.

MacMinn, C. W., Szulczewski, M. L., & Juanes, R. 2011. CO_2 migration in saline aquifers. Part 2. Capillary and solubility trapping. *Journal of Fluid Mechanics*, *688*, 321-351.

Maier, C., Schmid, K., Ahmed Elfeel, M. & Geiger, S. 2013. Multi-rate mass-transfer dual-porosity modeling using the exact analytical solution for spontaneous imbibition. SPE Paper 164926 presented the SPE Europec, London, 10-13 June.

Makel, 2007. The modelling of fractured reservoirs: constraints and potential for fracture network geometry and hydraulics analysis. Geological Society, London, Special Publications, **292**, 375-403.

Manrique, E. J., Muci, V. E. & Gurfinkel, M. E. 2007. EOR field experiences in carbonate reservoirs in the United States. *SPE Reservoir Evaluation & Engineering*, **10**(6), 667-686.

Matthai, S., Geiger, S., Roberts, S., et al. 2007. Numerical simulations of multiphase fluid flow in structurally complex reservoirs. Geological Society, London, Special Publications, **292**, 405–429.

Morrow, N. R., & Mason, G. 2001. Recovery of oil by spontaneous imbibition. *Current Opinion in Colloid & Interface Science*, *6*(4), 321-337.

Oda, M. 1985. Permeability tensor for discontinuous rock masses. Geotechnique, **35**(4), 483-495.

Okasha, T. M., Funk, J. J., & Al-Rashidi, H. N. 2007. Fifty years of wettability measurements in the Arab-D Carbonate Reservoir. Paper SPE 105114, presented at the 15th SPE Middle East Oil & Gas Conference, Bahrain, 11–14 March.

Oladyshkin, S., Class, H., Helmig, R., & Nowak, W. 2011. A concept for data-driven uncertainty quantification and its application to carbon dioxide storage in geological formations. *Advances in Water Resources*, **34**(11), 1508-1518.

Onwunalu, J. E. & Durlofsky, L. J. 2011. A new well-pattern-optimisation procedure for large-scale field development. *SPE Journal*, September, 594-607.

Petvipusit, K. R., Elsheikh, A. H., Laforce, T. C., King, P. R., & Blunt, M. J. 2014. Robust optimisation of CO_2 sequestration strategies under geological uncertainty using adaptive sparse grid surrogates. *Computational Geosciences*,*18*(5), 763-778.

Pierre, A., Durlet, C., Razin, P. & Chellai E. H. 2010. Spatial and temporal distribution of ooids along a Jurassic carbonate ramp: Amellago outcrop transect, High-Atlas, Morocco. Geological Society, London, Special Publication, **329**, 65-88.

Piri, M., & Blunt, M. J. 2005. Three-dimensional mixed-wet random pore-scale network modeling of two-and three-phase flow in porous media. I. Model description. *Physical Review E*, ***71***(2), 026301.

Pizarro, J. O. & Branco, C. C. 2012. Challenges in implementing an EOR project in the pre-salt province deep offshore Brasil. Paper SPE 155665 presented at the SPE EOR Conference at Oil and Gas West Asia, 16-18 April 2012, Muscat, Oman.

Pruess, K., Xu, T., Apps, J., & Garcia, J. 2003. Numerical modeling of aquifer disposal of CO2. *SPE Journal*, **8**(1), 49-60.

Qi, R., LaForce, T. C., & Blunt, M. J. 2008. Design of carbon dioxide storage in oil fields. In *SPE Annual Technical Conference and Exhibition*. Society of Petroleum Engineers.

Qi, R., LaForce, T. C., & Blunt, M. J. 2009. Design of carbon dioxide storage in aquifers. *International Journal of Greenhouse Gas Control*, *3*(2), 195-205.

Queipo, N. V., Haftka, R. T., Shyy, W., Goel, T., Vaidyanathan, R., & Kevin Tucker, P. 2005. Surrogate-based analysis and optimization. *Progress in aerospace sciences*, *41*(1), 1-28.

Ramirez, B., Kazemi, H., Al-Kobaisi, M., Ozkan, E. & Atan, S. 2009. A critical review for proper use of water/oil/gas transfer functions in dual-porosity naturally fractured reservoirs: Part I. *SPE Res. Eval & Eng*, **12**(2), 200-210.

Rawahi, A., Hafez, H., Al-yafei, A., Ghori, S., Putney, K., & Matthews, T. 2012. Maximize the Ultimate Recovery by Designing & Optimizing a CO2 Miscible Gas Injection Pilot in Giant Carbonate Oil Reservoir, Abu Dhabi. Paper SPE 162277 presented at the Abu Dhabi International Petroleum Conference and Exhibition, Abu Dhabi, 11-14 November.

Ryazanov A. V., van Dijke M. I. J. & Sorbie, K. S. 2009. Two-phase pore-network modelling: existence of oil layers during water invasion. *Transport in Porous Media*, **80**(1), 79–99.

Ryazanov A. V., van Dijke M. I. J. & Sorbie, K. S. 2010. Pore-network prediction of residual oil saturation based on oil layer drainage in mixed-wet systems. Paper SPE 129919 presented at the SPE Improved Oil Recovery Symposium, Tulsa, Oklahoma, 24-28 April.

Schmid, K. S., & Geiger, S. 2012. Universal scaling of spontaneous imbibition for water-wet systems. *Water Resources Research*, *48*(3).

Schmid, K. S., & Geiger, S. 2013. Universal scaling of spontaneous imbibition for arbitrary petrophysical properties: Water-wet and mixed-wet states and Handy's conjecture. *Journal of Petroleum Science and Engineering*, *101*, 44-61.

Shekhar, R., Sahni, I., Benson, G., et al. 2010. Sensitivities to flow-modelling assumptions for a heterogeneous carbonate ramp – an example from a Jurassic carbonate ramp. Paper K032 presented at 72nd EAGE conference & Exhibition incorporating SPE EUROPEC, Barcelona, Spain, 14-17 June.

Sohrabi, M., Kechut, N. I., Riazi, M., Jamiolahmady, M., Ireland, S., & Robertson, G. 2011. Safe storage of CO_2 together with improved oil recovery by CO_2 enriched water injection. *Chemical Engineering Research and Design*, **89(9)**, 1865-1872.

Spiteri, E. J. & Juanes, R. 2006. Impact of relative permeability hysteresis on numerical simulation of WAG injection. *Journal of Petroleum Science and Engineering*, **50**, 115-139.

Spiteri, E. J., Juanes, R., Blunt, M. J., & Orr, F. M. (2008). A new model of trapping and relative permeability hysteresis for all wettability characteristics.*Spe Journal*, *13*(03), 277-288.

Stone, H. L. 1973. Estimation of three-phase relative permeability and residual oil data. *Journal of Canadian Petroleum Technology*, **12**, 53.

Szulczewski, M. L., MacMinn, C. W., Herzog, H. J., & Juanes, R. 2012. Lifetime of carbon capture and storage as a climate-change mitigation technology. *Proceedings of the National Academy of Sciences*, *109*(14), 5185-5189.

Toublanc, A., Renaud, S., Sylte, J. E., Clausen, C. K., Eiben, T. & Nadland, G. 2005. Ekofisk Field: fracture permeability evaluation and implementation in the flow model. *Petroleum Geoscience*, **11**, 321-330.

Valvatne, P. H., & Blunt, M. J. 2004. Predictive pore-scale modeling of two-phase flow in mixed wet media. *Water Resources Research*, *40*(7).

Van Dijke, M. I. J., Sorbie, K. S., & McDougall, S. R. 2001. Saturation-dependencies of three-phase relative permeabilities in mixed-wet and fractionally wet systems. *Advances in Water Resources*, *24*(3), 365-384.

Warren, J. E. & Root, P. J. 1963. The behaviour of naturally fractured reservoirs. *SPE Journal*, **3** (3), 245-255.

Wei, L., Hadwin, J., Chaput, E., Rawnsley, K. & Swaby, P. 1998. Discriminating fracture patterns in fractured reservoirs by pressure transient tests. Paper SPE 49233, presented at the SPE Annual Technical Conference and Exhibition, New Orleans, Louisiana, 27-30 September.

Wildenschild, D., Armstrong, R. T., Herring, A. L., Young, I. M., & William Carey, J. 2011. Exploring capillary trapping efficiency as a function of interfacial tension, viscosity, and flow rate. *Energy Procedia*, **4**, 4945-4952.

Wilkinson, M., Haszeldine, R. S., Fallick, A. E., Odling, N., Stoker, S. J., & Gatliff, R. W. 2009. CO2–mineral reaction in a natural analogue for CO2 storage—implications for modeling. *Journal of Sedimentary Research,* **79**(7), 486-494.

Wriedt, J., Deo, M., Han, W. S., & Lepinski, J. 2014. A methodology for quantifying risk and likelihood of failure for carbon dioxide injection into deep saline reservoirs. *International Journal of Greenhouse Gas Control*, *20*, 196-211.